Applying the parameterising manifold approach to the wind-driven circulation

Henri van den Pol
Student Mathematical Sciences, Utrecht University

Abstract

Recently Chekroun et al. [4, 5] developed a method based on so called 'parameterising manifolds' to study stochastic (partial) differential equations. This method is promising for obtaining stochastic reduced models. We apply their method to a model of the wind-driven ocean ocean circulation at midlatitudes. To model the stream function ψ we use the quasi-geostrophic barotropic potential vorticity equation. The Reynolds number (R) is used as bifurcation parameter. ψ is susceptible to several types of bifurcations. We study the pitchfork bifurcation which occurs for $R \approx 36.6$.

We apply reduction methods to model perturbations around the stationary state. First the deterministic case is considered and the parameterising manifold approach is compared to the Galerkin type of method used in [16]. It is shown that the 'parameterising manifold' approach may be seen as an extension of the Galerkin method. To include also baroclinic effects, we model baroclinic instabilities by noise on the perturbations. The stochastic reduced model we obtain from the parameterising manifold approach captures the dynamics of the full stochastic model well.

Contents

1 The goal and research questions

The main aim of this thesis is to study with the newly developed stochastic model reduction methods by Chekroun et al[4, 5] as applied to a stochastic model of the wind-driven circulation.

We study the following research questions:

1. How does the parameterising manifold method perform compared to a Galerkin method in the deterministic case?
2. Are the stochastic reduced models capable of capturing important features of the full model?

The idea is to construct (numerically) a low-order (stochastic) amplitude equation model, modelling the perturbations around a stationary state.

2 Introduction

A lot of research has been done in the direction of dynamical systems, and the theory of invariant manifolds for ordinary differential equations (ODEs) and partial differential equations (PDEs) is well developed. A special kind of invariant manifolds are the inertial manifolds which are interesting because eventually all the solutions are attracted to this manifold.

Because of this fact, the dynamics of an high dimensional dynamical system can be studied by studying the dynamics of the low dimensional inertial manifold. In the deterministic case there are methods developed to obtain so called approximating inertial manifolds (AIMs). With use of such AIMs, one obtains reduced models which capture the dynamics of the full model. Studying an approximating inertial manifold is cheaper than studying the full model and might also give more insight in the important processes which take place.

However, contrary to the deterministic case, very few algorithms are available to compute stochastic AIMs in practice. In 2015, Chekroun et al [4, 5] introduced the so called 'parameterising manifolds' (PMs) as substitute for stochastic AIMs. We are interested in this method, because stochastic reduced models enable to study stochastic features as the probability density function (PDF) of the full stochastic model. PDFs might for example enable to predict bifurcations in the full stochastic model and with the use of PDFs we may be able to predict what kind of bifurcations will happen.

As a test problem the wind-driven ocean circulation is chosen, since it is known to be susceptible to several bifurcations. A simple model the wind-driven circulation is the quasi-geostrophic barotropic potential vorticity equation in an idealised ocean basin. We will refer to this model as 'the full model'. The Reynolds number is used as bifurcation parameter. We will consider here the article [16] where a deterministic reduced model is obtained for this problem and we will compare it with the deterministic parameterising manifold approach and see how the methods are connected.

As an example we will study the pitchfork bifurcation of the model. We consider reduced models based on the Galerkin approach of [16] and models based on parameterising manifolds to study perturbations around an unstable stationary state. We will show how to use both approaches. We show that the deterministic reduced models are able to capture the perturbations around the unstable stationary state. To incorporate baroclinic effects, we add baroclinic instabilities as a multiplicative noise term to our perturbations. We obtain therefore a stochastic (partial) differential equation for our perturbations. We will study the stochastic evolution equation for the perturbations by applying the stochastic reduction method based on PMs. We are able to capture the important features of the full model with the reduced model.

3 Physics of the problem

We consider an ocean flow with constant density (ρ) in a rectangular basin of horizontal dimensions L and B and with constant depth D, which is situated on a midlatitude β-plane with Coriolis parameter $f = f_0 + \beta_0 y$. The ocean circulation in the basin is forced at the surface through a wind stress vector $\tau = \tau_0\ (\tau^x(x,y), \tau^y(x,y))$.

3.1 The quasi-geostrophic model

In a quasi-geostrophic approximation, the flow can be modelled by the well-known barotropic vorticity equation (Pedlosky, 1987) for the geostrophic streamfunction ψ. This equation is non-dimensionalized by using horizontal and vertical length scales L and D, a characteristic horizontal velocity scale U, a time scale L/U and the maximum amplitude of the wind stress τ_0. With the introduction of the horizontal velocities u and v and the relative vorticity ζ, the dimensionless model can be written as:

$$\left[\frac{\partial}{\partial t} + u\frac{\partial}{\partial x} + v\frac{\partial}{\partial y}\right](\zeta - F\psi + \beta y) = R^{-1}\nabla^2\zeta + \alpha_\tau\left(\frac{\partial \tau^y}{\partial x} - \frac{\partial \tau^x}{\partial y}\right), \tag{1a}$$

$$\zeta = \nabla^2\psi, \tag{1b}$$

$$u = -\frac{\partial \psi}{\partial y}\ ,\ v = \frac{\partial \psi}{\partial x}. \tag{1c}$$

See [7, Eq. (5.90)] for its total form and a derivation of the formula. Note that in the above equation we do not consider bottom friction and bottom deformations. On the zonal boundaries ($x = 0$ and $x = 1$) no-slip conditions and a Munk boundary layer are prescribed, whereas at the meridional boundaries ($y = 0$ and $y = A$), we apply slip conditions and we do not have a boundary layer:

$$x = 0, x = 1, \qquad \psi = 0, \frac{\partial \psi}{\partial x} = 0, \tag{2a}$$

$$y = 0, y = A, \qquad \psi = 0, \zeta = 0. \tag{2b}$$

Besides the aspect ratio $A = B/L$, several other parameters appear, i.e. the Reynolds number R, the strength of the planetary vorticity gradient β, the wind stress forcing strength α_τ and the Froude number F. The parameters are defined as

$$R = \frac{UL}{A_H},\ \beta = \frac{\beta_0 L^2}{U},\ \alpha_\tau = \frac{\tau_0 L}{\rho D U^2},\ F = \frac{f_0^2 L^2}{gD}. \tag{3}$$

where A_H is the lateral friction coefficient (the width of the Munk boundary layer depends on this coefficient). A consequence of increasing Reynolds number is that A_H decreases and that we therefore have that the Munk boundary layer becomes smaller.

The characteristic velocity U is chosen such that $\alpha_\tau = \beta$ to give Sverdrup flow (i.e. such that $\beta\frac{\partial \psi}{\partial x}$ balances $\alpha_\tau\left(\frac{\partial \tau^y}{\partial x} - \frac{\partial \tau^x}{\partial y}\right)$) over the main part of the basin. A Sverdrup solution everywhere on the basin is plotted in figure 1. The figure is from [7, Figure 6.4]

The wind stress considered is

$$\tau^x(y) = -\frac{1}{2\pi}((1-a)\cos(\frac{2\pi y}{A}) - a\sin(\frac{2\pi y}{A})),\ \tau^y = 0, \tag{4}$$

where the parameter a controls the asymmetry of the wind stress field with respect to the mid-axis of the basin. A plot of $\tau^x(y)$ where $a = 0$ and $A = 1$ is given in figure 2.

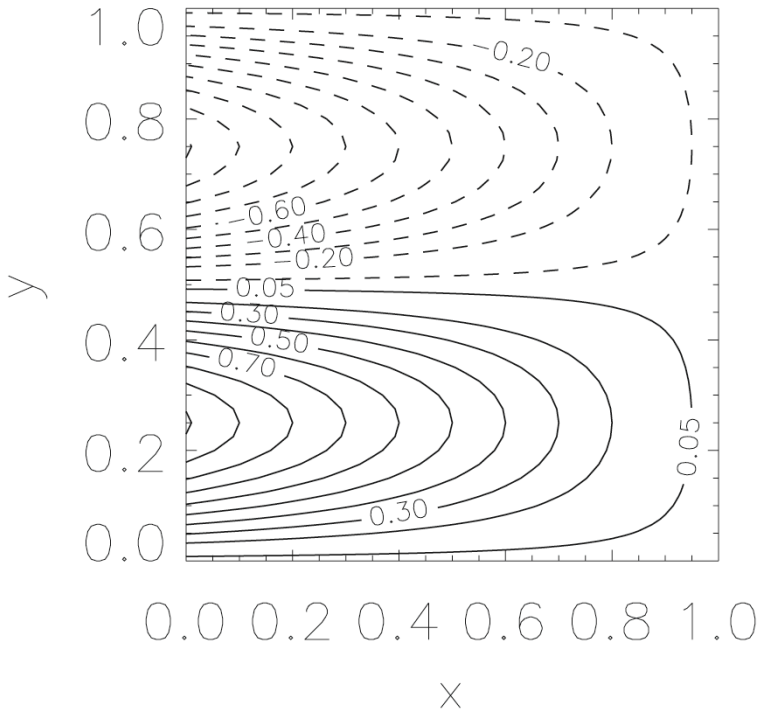

Figure 1: Contourplot of the Sverdrup solution where $a = 0$ and $A = 1$.

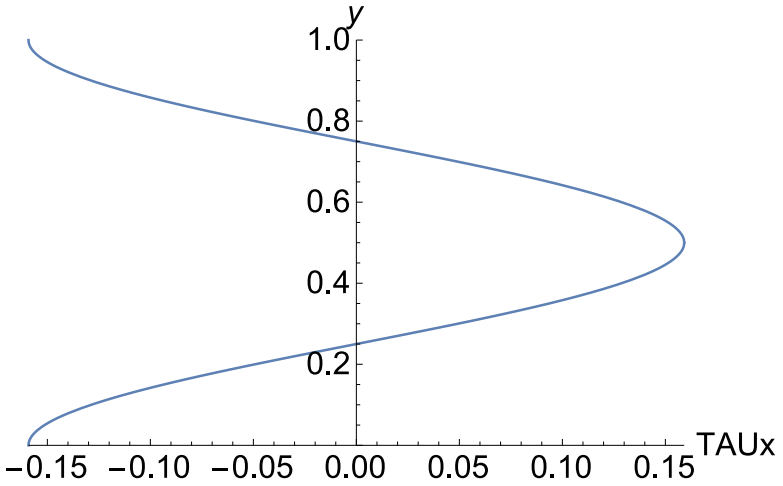

Figure 2: Plot of $\tau^x(y)$ where $a = 0$ and $A = 1$.

The unforced ($\alpha_\tau = 0$) system of equations and boundary conditions admits a reflection symmetry through the mid-axis ($y = A/2$) of the basin. This reflection $\mathcal{R}$ has representation

$$\mathcal{R}(\psi(x, A - y)) = -\psi(x, y). \tag{5}$$

For $a = 0$, the applied wind stress admits a similar symmetry and this places constraints on the bifurcations, i.e. symmetry breaking bifurcations will be of pitchfork type [11].

3.2 Stationary solutions and their stability

We can rewrite the left side of equation (1) as:

$$\frac{\partial}{\partial t}(\nabla^2\psi - F\psi) - \frac{\partial\psi}{\partial y}\frac{\partial}{\partial x}(\nabla^2\psi - F\psi) + \frac{\partial\psi}{\partial x}\frac{\partial}{\partial y}(\nabla^2\psi - F\psi) + \beta\frac{\partial\psi}{\partial x}.$$

Therefore (1) is rewritten as:

$$(\nabla^2 - F)\frac{\partial\psi}{\partial t} = (R^{-1}\nabla^4 - \beta\frac{\partial}{\partial x})\psi + \frac{\partial\psi}{\partial y}\frac{\partial}{\partial x}(\nabla^2\psi - F\psi) - \frac{\partial\psi}{\partial x}\frac{\partial}{\partial y}(\nabla^2\psi - F\psi) + \alpha_\tau\left(\frac{\partial\tau^y}{\partial x} - \frac{\partial\tau^x}{\partial y}\right). \quad (6)$$

We can now write the above equation in the following form:

$$\mathcal{M}\frac{\mathrm{d}\psi}{\mathrm{d}t} = L_\lambda\psi + B(\psi,\psi) + f,$$

where the linear operators $\mathcal{M}, L_\lambda$ are given by:

$$\mathcal{M} = \nabla^2 - F, \quad (7a)$$

$$L_\lambda = R^{-1}\nabla^4 - \beta\frac{\partial}{\partial x}. \quad (7b)$$

We will write L_λ, because λ is one of the bifurcation parameters (R, β). The bilinear operator $B(\psi,\psi)$ and the forcing f are given by:

$$B(\psi,\psi) = \frac{\partial\psi}{\partial y}\frac{\partial}{\partial x}(\nabla^2\psi - F\psi) - \frac{\partial\psi}{\partial x}\frac{\partial}{\partial y}(\nabla^2\psi - F\psi), \quad (8a)$$

$$f = \alpha_\tau\left(\frac{\partial\tau^y}{\partial x} - \frac{\partial\tau^x}{\partial y}\right). \quad (8b)$$

We will use $F = 0$ for the simulations. With $F = 0$ equation (6) can be simplified and it can be written as the following system of equations:

$$\frac{\partial}{\partial t}\zeta = R^{-1}\nabla^2\zeta - \beta\frac{\partial}{\partial x}\psi + \frac{\partial\psi}{\partial y}\frac{\partial}{\partial x}\zeta - \frac{\partial\psi}{\partial x}\frac{\partial}{\partial y}\zeta + \alpha_\tau\left(\frac{\partial\tau^y}{\partial x} - \frac{\partial\tau^x}{\partial y}\right), \quad (9a)$$

$$\zeta = \Delta\psi. \quad (9b)$$

If we define $\phi = (\zeta,\psi)^T$, $K(\zeta,\psi) = K(\phi) = \psi_y\zeta_x - \psi_x\zeta_y$ and

$$\mathcal{M} = \begin{bmatrix}1 & 0\\ 0 & 0\end{bmatrix}, \quad L_\lambda = \begin{bmatrix}\frac{1}{Re}\Delta & -\beta\frac{\partial}{\partial x}\\ -1 & \Delta\end{bmatrix}, \quad B(\phi,\phi) = \begin{pmatrix}K(\phi)\\ 0\end{pmatrix}, \quad f = \begin{pmatrix}\alpha_\tau\left(\frac{\partial\tau^y}{\partial x} - \frac{\partial\tau^x}{\partial y}\right)\\ 0\end{pmatrix}. \quad (10)$$

The system of equations 9 can be rewritten as:

$$\mathcal{M}\frac{\partial\phi}{\partial t} = L_\lambda\phi + B(\phi,\phi) + f, \quad (11)$$

Here $\mathcal{M}$ is a singular linear operator, L_λ is a linear operator, B is a bilinear operator and f is the forcing.

Systems (6) and (11) are in principle equivalent if $F = 0$, but system (11) is from a numerical point of view more practical, because one does not have to implement higher order boundary conditions for ψ. So we will use

this system for the computations.

Equation (11) is discretised in the spatial domain using central differences on an equidistant $N \times M$ grid. After discretisation we obtain from equation (9a) a system of bilinear differential equations, and because equation (9b) has no derivatives with respect to time, we will refer to these equations as algebraic equations.

To simplify the presentation, we will still keep the same notations when a discretized version of Eq. (11) will be considered, i.e. a discretisation $\mathcal{M}_{N\times M}$ of $\mathcal{M}$, will be still denoted by $\mathcal{M}$, etc. So we write our discretised system as:

$$\mathcal{M}\frac{\partial \phi}{\partial t} = L_\lambda \phi + B(\phi, \phi) + f. \tag{12}$$

Now $\phi = (\zeta, \psi)^T$ is the d-dimensional state vector ($d = 2 \times N \times M$), consisting of the unknowns at each gridpoint. $\mathcal{M}$ is a singular linear map from $\mathbb{R}^d \to \mathbb{R}^d$, the operator L_λ is a linear map from $\mathbb{R}^d \times \mathbb{R} \to \mathbb{R}^d$, B is a bilinear map from $\mathbb{R}^d \times \mathbb{R}^d \to \mathbb{R}^d$, and the forcing $f \in \mathbb{R}^d$.

Stationary solutions $\Phi_{\lambda,f}$ satisfy:

$$\frac{\mathrm{d}\Phi_{\lambda,f}}{\mathrm{d}t} = 0 \implies L_\lambda \Phi_{\lambda,f} + B(\Phi_{\lambda,f}, \Phi_{\lambda,f}) + f = 0, \tag{13}$$

which is a system of d bilinear algebraic equations. Note that we use the notation $\Phi_{\lambda,f}$ to denote that the stationary state depends on the bifurcation parameter λ and the forcing f.

For computing a branch of stationary solutions in one of the bifurcation parameters we use a pseudo-arclength method[12]. We use a Newton-Raphson method to converge to the branch of stationary solutions. The linear systems are solved with a preconditioned conjugate gradient method [15]. The same method as in [16] is used, we refer to that paper for more details.

If a stationary solution is determined, a linear stability analysis is done and bifurcations like pitchfork, limit points and Hopf can be detected. For the linear stability analysis we have to solve the generalised eigenvalue problem:

$$\gamma \mathcal{J}\Phi_{\lambda,f} = \kappa \mathcal{M}\Phi_{\lambda,f}, \tag{14}$$

Here $\mathcal{J}$ is the Jacobian matrix of the right hand side of (12) and $\mathcal{M}$ is the same as in equation (12). We solve the problem using a QZ method [10]. If $\gamma \neq 0$ then we will denote an eigenvalue of the problem by $\sigma = \kappa/\gamma$.

4 Deterministic Galerkin approach

In this section we explain the approach used in [16]. Let $\Phi_{\lambda,f}$ be a stationary solution and let $v(t)$ be a perturbation to the stationary state. We can write $\phi(t) = \Phi_{\lambda,f} + v(t)$. If we substitute $\phi(t) = v(t) + \Phi_{\lambda,f}$ in equation (12), we obtain for the left hand side of equation (12):

$$\mathcal{M}\frac{\mathrm{d}(v + \Phi_{\lambda,f})}{\mathrm{d}t} = \mathcal{M}\frac{\mathrm{d}v}{\mathrm{d}t}.$$

For the right hand side we get:

$$L_\lambda(v + \Phi_{\lambda,f}) + B(v + \Phi_{\lambda,f}, v + \Phi_{\lambda,f}) + f =$$

$$L_\lambda v + B(v, \Phi_{\lambda,f}) + B(\Phi_{\lambda,f}, v) + B(v, v) + L_\lambda \Phi_{\lambda,f} + B(\Phi_{\lambda,f}, \Phi_{\lambda,f}) + f.$$

$\Phi_{\lambda,f}$ is a stationary state, hence the last three terms on the right side of the above equation sum to zero. Therefore we get that the expression for the right hand side simplifies to:

$$L_\lambda v + B(v, \Phi_{\lambda,f}) + B(\Phi_{\lambda,f}, v) + B(v, v).$$

Now, given a stationary state $\Phi_{\lambda,f}$, we define the following linearized operator,

$$\mathcal{J}_{\lambda,f}\cdot = L_{\lambda,f}\cdot + B(\Phi_{\lambda,f}, \cdot) + B(\cdot, \Phi_{\lambda,f}), \tag{15}$$

such that we can rewrite the right hand side as:

$$\mathcal{J}_{\lambda,f} v + B(v, v).$$

Now we see that the evolution equation satisfied by the perturbations v around the stationary state $\Phi_{\lambda,f}$, is:

$$\mathcal{M}\frac{\mathrm{d}v}{\mathrm{d}t} = \mathcal{J}_{\lambda,f} v + B(v, v). \tag{16}$$

Here $\mathcal{J}_{\lambda,f}$ is a linear operator and B is a bilinear operator. We assume $\mathcal{J}_{\lambda,f}$ has only simple eigenvalues. In this case the linear operator $\mathcal{J}_{\lambda,f}$ has an eigenvector decomposition:

$$\mathbf{L}^H \mathcal{J}_{\lambda,f}\mathbf{R} = \mathbf{\Sigma}\ ;\ \mathbf{L}^H \mathcal{M}\mathbf{R} = \mathbf{I} \tag{17}$$

Here $\mathbf{R}$ and $\mathbf{L}$ denote the right and left hand eigenspaces of the linear operator $\mathcal{J}_{\lambda,f}$, $\mathbf{I}$ is the identity and the diagonal matrix $\mathbf{\Sigma}$ contains the corresponding eigenvalues, i.e.,

$$\mathbf{R} = \begin{pmatrix}\mathbf{r}_1 & \mathbf{r}_2 & \cdots & \mathbf{r}_r\end{pmatrix}, \tag{18a}$$

$$\mathbf{L} = \begin{pmatrix}\mathbf{l}_1 & \mathbf{l}_2 & \cdots & \mathbf{l}_r\end{pmatrix}, \tag{18b}$$

$$\mathbf{\Sigma} = \mathrm{diag}(\sigma_1 \quad \sigma_2 \quad \cdots \quad \sigma_r), \tag{18c}$$

where $r = rank(\mathbf{\Sigma}) = (M-2)\times(N-2) < d$; the latter inequality is due to the singular nature of $\mathcal{M}$ and the boundary conditions on ψ. Relation (17) states that we can diagonalise $\mathcal{J}_{\lambda,f}$ by use of its eigenvectors. Because the matrix $\mathcal{M}$ is simply a kind of identity matrix (see (10)), $\mathbf{L}^H\mathcal{M}\mathbf{R} = \mathbf{I}$ follows from the fact that $\mathbf{L}$ and $\mathbf{R}$ are a bi-orthogonal set of eigenvectors. These properties will be used in the Galerkin projection below.

With the use of this eigenbasis, we consider now the case where the perturbation v is expanded in m righthand eigenvectors: (One could equivalently say we project v on the space spanned by the first m eigenvectors)

$$v(t) = \mathbf{R}_m \boldsymbol{a}(t) = \sum_{j=1}^{m} \mathbf{r}_j a_j(t). \tag{19}$$

The matrix $\mathbf{R}_m$ denotes the $m-$dimensional subspace of $\mathbf{R}$ of suitably chosen righthand vectors, and $\mathbf{L}_m$ is its adjoint subspace.

Substitution of (19) into (16) yields:

$$\mathcal{M}\mathbf{R}_m \frac{d\boldsymbol{a}}{dt} = \mathcal{J}_{\lambda,f}\mathbf{R}_m\boldsymbol{a} + B(\mathbf{R}_m\boldsymbol{a}, \mathbf{R}_m\boldsymbol{a}). \tag{20}$$

Projection onto the lefthand eigenbasis $\mathbf{L}_m$ and the use of the relations (17), results in the set of coupled amplitude equations:

$$\frac{d\boldsymbol{a}}{dt} = \Sigma_m\boldsymbol{a} + b(\boldsymbol{a}, \boldsymbol{a}). \tag{21a}$$

The operators in this projected system are defined as:

$$\Sigma_m = \mathbf{L}_m^H \mathcal{J}_{\lambda,f}\mathbf{R}_m, \tag{21b}$$

$$b(\boldsymbol{a}, \boldsymbol{a}) = \mathbf{L}_m^H B(\mathbf{R}_m\boldsymbol{a}, \mathbf{R}_m\boldsymbol{a}), \tag{21c}$$

with Σ_m the diagonal matrix containing the eigenvalues corresponding to the eigenvectors of $\mathbf{R}_m$. In terms of the individual components, the evolution of amplitude $a_j(t)$ is governed by:

$$\frac{da_j}{dt} = \sigma_j a_j + \sum_{k=1}^{m}\sum_{l=1}^{m} B_{kl}^j a_k a_l, \qquad j = 1, \ldots, m. \tag{22a}$$

The coefficients B_{kl}^j are defined as:

$$B_{kl}^j = \mathbf{l}_j^H B(\mathbf{r}_k, \mathbf{r}_l). \tag{22b}$$

Note that these coefficients depend implicitly upon λ and f, on which the spectral problem (17) relies via $\mathcal{J}_{\lambda,f}$.

We will use a Crank-Nicholson scheme to discretise equation (22) in time and we use a Newton-Raphson method to solve the resulting set of nonlinear algebraic equations.

5 Parameterising manifolds for bilinear PDEs: the non-self adjoint and singular case

The method of [16] has a drawback: the perturbation considered is only in the direction of the first m eigenvectors. In the parameterising manifold approach the idea is to look for a perturbation in the direction of all the eigenvectors. If one then looks at the equations for the amplitudes of the first m eigenvectors ('the resolved amplitudes') these equations will then not only contain the first m amplitudes, but also 'unresolved amplitudes'. With help of a parameterising manifold the unresolved amplitudes are modelled by (and in terms of) the resolved amplitudes. The expression we obtain in this way is substituted back in the evolution equation for the resolved amplitudes and so we are able to obtain an approximation for the perturbation v.

We order the eigenvalues by their real part. So we will have $Re[\sigma_1] \geq Re[\sigma_2] \geq Re[\sigma_3] \geq \ldots$. $\mathbf{r}_i$ and $\mathbf{l}_i$ are the right and left eigenvector belonging to eigenvalue σ_i. We denote by $\mathcal{H}^c$ the space spanned by the m first eigenvectors. The projection of the perturbation v on this space is denoted by v_c: v_c are the 'resolved variables'. We can write $v_c = \mathbf{R}_m \mathbf{a}_m = \sum_{i=1}^{m} a_i \mathbf{r}_i$, where a_i denote the amplitude of eigenvector $\mathbf{r}_i$. We denote by $\mathcal{H}^s$ the space spanned by the $m+1$-th until r-th eigenvector. The projection of v on $\mathcal{H}^s$ is denoted by v_s: v_s are the 'unresolved variables'. We can write $v_s = \mathbf{R}_{r-m} \mathbf{a}_{r-m} = \sum_{i=m+1}^{r} a_i \mathbf{r}_i$.

The PDE (11) has infinitely many eigenvectors. If we would not discretise our space then we could also obtain a PDE for our perturbation v. Infinitely many eigenvalues means $r = \infty$. In this case we have that $\mathcal{H}^c$ together with $\mathcal{H}^s$ span the entire space and therefore we can write every v as $v = v_c + v_s$. [5, Eq. (2.13)]. In a discretised system the number r of eigenvalues and eigenvectors is finite and therefore we only look at perturbations which can be written as a linear combination of maximum r eigenvectors. Therefore $v = v_c + v_s = \mathbf{R}_r \mathbf{a}_r = \sum_{i=1}^{r} a_i \mathbf{r}_i$.

To parameterise unresolved variables by resolved variables we use backward-forward systems which are partially coupled. We use a backward-forward system in the following way: we integrate the linear part of the equation for the resolved variables first backward and we use this outcome to integrate the equation for the unresolved variables forward. For the forward integration we let the unresolved variables depend on the resolved variables through the nonlinear terms. We do not couple the output of the unresolved equations back to the resolved equations, therefore we call it partially coupled.

To incorporate the baroclinic instabilities, we add them as a multiplicative noise term on the perturbation v. Therefore Eq. (16) incorporates a multiplicative noise as follows,

$$\mathcal{M}\mathrm{d}v = \big(\mathcal{J}_{\lambda,f} v + B(v,v)\big)\mathrm{d}t + \delta \mathcal{M} v \circ \mathrm{d}W_t. \tag{23}$$

Here W_t denotes a one-dimensional Wiener process, $v \circ \mathrm{d}W_t$ is understood in the Stratonovich sense, and $\delta \geq 0$ quantifies the intensity of that noise term.

5.1 General approach to obtain a parameterising manifold

Given λ in $\mathbb{R}$ and a forcing f in $\mathcal{H}$, a nonlinear parameterising manifold function $h^{(1)}_{\lambda,f} : \mathcal{H}^{\mathfrak{c}} \to \mathcal{H}^{\mathfrak{s}}$ can be obtained from backward-forward system which are associated with Eq. (16). Rigorous studies from [5, Sect. 4.5] and from [4, Chaps. 6 & 7] help support the idea that the graph of such a function can actually provide, even in the present context, a *parameterising manifold*, as long as we are not too far from the criticality.

To obtain a parameterising manifold h^1 for our model, we consider the following backward-forward system of [5, Eq. (4.1 a-c)] which we modified so that it fits our problem. Here the u_c is an approximation of the resolved

variables v_c and the u_s give an approximation of the unresolved variables v_s. We want to approximate $v_s(t)$ in terms of $v_c(t)$:

$$\mathrm{d}u_c = \mathcal{J}^c_{\lambda,f} u_c \mathrm{d}s + \delta u_c \circ \mathrm{d}W_s, \qquad s \in [-T, 0], \tag{24a}$$

$$\mathrm{d}u_s = \left(\mathcal{J}^s_{\lambda,f} u_s + P_s B[u_c(s-T), u_c(s-T)]\right) \mathrm{d}s + \delta u_s \circ \mathrm{d}W_s, \qquad s \in [0, T], \tag{24b}$$

with $u_c(0) = \xi = v_c(t) \in \mathcal{H}^c$ and $u_s(0) = 0$ and P_s, P_c the projections on $\mathcal{H}^s$ and $\mathcal{H}^c$ respectively. $\mathcal{J}^c_{\lambda,f}$, $\mathcal{J}^s_{\lambda,f}$ are defined as $\mathcal{J}_{\lambda,f} P_c$ and $\mathcal{J}_{\lambda,f} P_s$ respectively. In the above equation W_t denotes a one-dimensional Wiener process, $\circ \mathrm{d}W_t$ is understood in the Stratonovich sense, and $\delta \geq 0$ quantifies the intensity of the noise term.

Remark: we expect that the v_c are also affected by the v_s, therefore we will model with our parameterising manifold the modes v_s which affect the v_c.

We consider a model only in our resolved variables. However if integrating the resolved variables would give an enormous contribution to the equation for the unresolved variables (so if $B(u_c, u_c)$ is big), then these resolved variables grow enormously and it should be important to consider these unresolved variables in our equation for the resolved variables. Therefore a parameterising manifold determines which unresolved variable are affected much by the resolved variables, and it parameterises these variables in terms of the resolved variables. So it looks in the history how the unresolved variables are affected by the resolved variables.

If we now take the limit for $T \to \infty$ then we get the parameterising manifold h^1 [5, Prop. 4.1 and Eq. (4.43)]:

$$h^1(\xi) = \lim_{T \to +\infty} u_s[\xi] = \int_{-\infty}^{0} e^{\delta W_s} e^{-s\mathcal{J}^s_{\lambda,f}} P_s B(e^{s\mathcal{J}^c_{\lambda,f}}\xi, e^{s\mathcal{J}^c_{\lambda,f}}\xi) ds, \tag{25}$$

where u_s solves equation (24b). This limit exists if $\sigma_{m+1} < k\sigma_m$ in the case where we have that the nonlinear term is k-linear (so in our case we have $k = 2$) [4, Eq. (6.27)]. This condition is always met if the eigenvalues of the eigenvectors in $\mathcal{H}^c$ are all greater or equal to zero. The parameterising manifold $h^1(\xi) = h^1(v_c)$ gives an approximation of v_s in v_c.

If $\mathcal{J}_{\lambda,f}$ is self-adjoint a necessary and sufficient condition for the above integral to exist is the following cross non-resonance condition: $\forall (i_1, i_2) \in (1, ..., m)^2, n > m$ it holds that:

$$(B^n_{i_1,i_2} \neq 0) \implies (\sigma_{i_1} + \sigma_{i_2} - \sigma_n > 0)\,. \tag{26}$$

The non-resonance condition is checked by our model. It is shown in [4, Cor. 6.1] that in the case where $\mathcal{J}_{\lambda,f}$ is self-adjoint that then h^1 can be decomposed as:

$$h^1(\xi) = \sum_{n=m+1}^{\infty} h^{(1),n}_{\lambda,f}(\xi) \mathbf{r}_n, \tag{27}$$

and for $n \geq m + 1$:

$$h^{(1),n}_{\lambda,f}(\xi) = \sum_{i_1,i_2=1}^{m} B^n_{i_1,i_2} M^{i_1,i_2}_n \xi_{i_1} \xi_{i_2},$$

with M^{i_1,i_2}_n given by:

$$M^{i_1,i_2}_n = \int_{-\infty}^{0} e^{(\sigma_{i_1} + \sigma_{i_2} - \sigma_n)s + \delta W_s} \mathrm{d}s. \tag{28}$$

This integral is well-defined because of the above cross non-resonance condition and the sub linear growth property of the Wiener process.

The $M_n^{i_1,i_2}$ term corresponds to the unique stationary solution of the SDE given in the equation below [4, Eq. 5.26]. This simplifies the computation in practice:

$$\mathrm{d}M = \Big(1 - \Big(\sigma_{i_1} + \sigma_{i_2} - \sigma_n\Big)M\Big)\,\mathrm{d}t - \delta M \circ \mathrm{d}W_t. \tag{29}$$

The integration of this equation should be performed simultaneously with the integration of the system (23), for a fixed realization ω of the noise. If $\mathcal{J}_{\lambda,f}$ is self-adjoint and the noise is set to zero ($\delta = 0$) we can evaluate the integral above and the M_n terms are then given by:

$$M_n^{i_1 i_2} = \frac{1}{\sigma_{i_1} + \sigma_{i_2} - \sigma_n}. \tag{30}$$

In the case we consider, $\mathcal{J}_{\lambda,f}$ is not self-adjoint, but it is believed by M.D. Chekroun [1] that we still should be able to follow the approach as explained above and that this will give good results. We will show that the method of backward-forward integration of [5, 2] can be adapted to the present context, in which $\mathcal{J}_{\lambda,f}$ is not self-adjoint and $\mathcal{M}$ is a singular operator, cases that were not addressed in [5, 2].

The question may arise how to set up the systems for the resolved and unresolved equations to get a good parameterising manifold. The system above is the simplest system giving parameterising manifold h^1. An example of more complex systems are systems where we need to integrate n-times backward before integrating forward; this gives access to the parameterising manifolds h^n. Details on how to do this are discussed in [5, Sect. 4.3].

In chapter 7 of [5] a two-layer backward-forward system is described which can be used in the case where no analytic expression for a parameterising manifold is available. In this case, the vector field of the above equations is built simultaneously with $v_c(t; w)$, as the time t evolves. The parameterising manifold function is thus computed "on the fly." This procedure is described in detail in [5, Chap. 7] by way of an example, where the parameterising manifold considered is $h^2(\xi)$. We implemented this two-layer backward forward system which is computed on the fly. For the results see section 9.2.3.

5.2 Obtaining a parameterising manifold for our model

Expanding v in r eigenvectors gives $v = \sum_{i=1}^{r} a_i \mathbf{r}_i = \mathbf{R}_r \mathbf{a}_r$. Substituting this in equation (16) and multiplying by $\mathbf{L}_r^H$ gives:

$$\mathrm{d}a_j = \left[\sigma_j a_j + \mathbf{l}_j^H B(\mathbf{R}_r\mathbf{a}_r, \mathbf{R}_r\mathbf{a}_r)\right]\mathrm{d}t + \delta a_j \circ \mathrm{d}W_t, \qquad j = 1, \ldots, r. \tag{31}$$

We can split this in equations for the resolved amplitudes and the unresolved amplitudes. We consider the following system (where the $\tilde{a}_k$ are approximations of a_k):

$$\mathrm{d}\tilde{a}_i = \sigma_i \tilde{a}_i \mathrm{d}s + \delta \tilde{a}_j \circ \mathrm{d}W_s, \qquad i = 1, \ldots, m, \qquad s \in [t-T, t],$$
$$\tilde{a}_i(t) = \xi = a_i(t), \qquad i = 1, \ldots, m.$$

Note that specifying the amplitudes $a_i(t)$ for all the m resolved amplitudes is the same as giving $v_c(t)$. These are the equations for the approximation of the resolved amplitudes. We integrate these equation first backward and substitute them in the next equation.

The equations for the approximation of the unresolved amplitudes are:

$$\mathrm{d}\tilde{a}_j = \left[\sigma_j \tilde{a}_j + \mathbf{l}_j^H B(\mathbf{R}_m\tilde{\mathbf{a}}_m, \mathbf{R}_m\tilde{\mathbf{a}}_m)\right]\mathrm{d}s + \delta \tilde{a}_j \circ \mathrm{d}W_s, \qquad j = m+1, \ldots, r, \qquad s \in [t-T, t],$$
$$\tilde{a}_j(t-T) = 0, \qquad j = m+1, \ldots, r.$$

These equations are integrated forward. From these systems we can obtain the $\tilde{a}_j(t)$ for $m+1 \leq j \leq r$ in terms of the $a_i(t)$ with $1 \leq i \leq m$. This means that we have (at time t) an approximation of our unresolved amplitudes in terms of our resolved amplitudes. This expression of course still involves our integration time T.

We have that:

$$\sum_{j=m+1}^{r} a_j(t)\mathbf{r}_j = v_s \approx u_s = \sum_{j=m+1}^{r} \tilde{a}_j(t)\mathbf{r}_j,$$

$$h^1[v_c(t)] = \lim_{T\to\infty} u_s[v_c(t)] = \lim_{T\to\infty} \sum_{j=m+1}^{r} \tilde{a}_j(t)\mathbf{r}_j = \sum_{j=m+1}^{r} h^{(1),j}_{\lambda,f}(\mathbf{a}_m)\mathbf{r}_j,$$

where $h^{(1),j}_{\lambda,f}$ is a polynomial of degree two. Note that $h^{(1),j}_{\lambda,f}(\mathbf{a}_m) = \tilde{a}_j \approx a_j$ and that letting $T \to \infty$ means that we take the whole history of the $\tilde{\mathbf{a}}$ into account.
Hence the resolved amplitudes are given by: (we write $B(x,x)$ as $B(x)$ for ease of notation)

$$\mathrm{d}a_j = \left[\sigma_j a_j + \mathbf{l}_j^H B\left(v_c + u_s\right)\right]\mathrm{d}t + \delta a_j \circ \mathrm{d}W_t, \qquad j = 1,\ldots,m.$$

If the limit for $T \to \infty$ converges we have:

$$\mathrm{d}a_j = \left[\sigma_j a_j + \mathbf{l}_j^H B\left(\sum_{i=1}^{m} a_i\mathbf{r}_i + \sum_{k=m+1}^{r} h^{(1),k}_{\lambda,f}(\mathbf{a}_m)\mathbf{r}_k\right)\mathbf{r}_k\right]\mathrm{d}t + \delta a_j \circ \mathrm{d}W_t, \qquad j = 1,\ldots,m.$$

If the limit for $T \to \infty$ does not converge we integrate back for a finite time T, so if we have $v_c(t)$ we can get a numerical expression for $u_s(t)$ and use this to calculate $v_c(t+\Delta t)$, et cetera.

5.2.1 Deterministic example of a PM with v_c and v_s spanned by one eigenvector

We consider the case $m = 1$ and $q = 2$, with $v = a_1\mathbf{r}_1 + a_2\mathbf{r}_2$ and $v_c = a_1\mathbf{r}_1$, $v_s = a_2\mathbf{r}_2$:

$$\frac{\partial a_1}{\partial t} = \sigma_1 a_1 + \mathbf{l}_1^H B(a_1\mathbf{r}_1 + a_2\mathbf{r}_2),$$
$$\frac{\partial a_2}{\partial t} = \sigma_2 a_2 + \mathbf{l}_2^H B(a_1\mathbf{r}_1 + a_2\mathbf{r}_2).$$

As as reduction we only consider our resolved amplitudes:

$$\frac{\partial a_1}{\partial t} = \sigma_1 a_1 + \mathbf{l}_1^H B(a_1\mathbf{r}_1 + a_2\mathbf{r}_2), \qquad t > 0.$$

Let's say we have $a_1(t) = \xi$. The above equation still contains $a_2(t)$; we use our parameterising manifold to obtain an approximation of a_2 in terms of a_1. For obtaining our parameterising manifold we consider the following backward-forward model:

$$\frac{\partial \tilde{a}_1}{\partial s} = \sigma_1 \tilde{a}_1, \qquad s \in [t-T, t],$$
$$\frac{\partial \tilde{a}_2}{\partial s} = \sigma_2 \tilde{a}_2 + \tilde{a}_1^2 \mathbf{l}_2^H B(\mathbf{r}_1), \qquad s \in [t-T, t],$$
$$\tilde{a}_1(t) = \xi = a_1(t), \qquad \tilde{a}_2(t-T) = 0.$$

We integrate the first equation backward and the second equation forward. In figure 3 is a schematic overview of this backward-forward system.

Solving the first equation gives:

$$\tilde{a}_1(s) = \xi e^{\sigma_1(s-t)}.$$

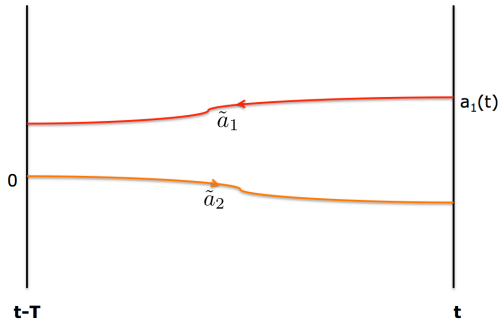

Figure 3: Schematic view of the backward-forward procedure. We integrate $\tilde{a}_1$ back from initial point $\tilde{a}_1(t) = a_1(t)$ to obtain all values $\tilde{a}_1$ in the interval $[t-T, t]$. We use these values in the equation for $\tilde{a}_2$ which we integrate from $\tilde{a}_2(t-T) = 0$ to $\tilde{a}_2(t)$.

Substituting this in the second equation gives:

$$\frac{\partial \tilde{a}_2}{\partial s} = \sigma_2 \tilde{a}_2 + e^{2\sigma_1(s-t)}\xi^2 B_{1,1}^2, \qquad s \in [t-T, t].$$

Solving this with variation of constants gives:

$$\tilde{a}_2(s) = Ce^{\sigma_2 s} + \frac{\xi^2 B_{1,1}^2}{2\sigma_1 - \sigma_2} e^{2\sigma_1(s-t)}, \qquad s \in [t-T, t].$$

We impose the condition at $t-T$ and so we obtain:

$$\tilde{a}_2(s) = \frac{\xi^2 B_{1,1}^2}{2\sigma_1 - \sigma_2}(e^{2\sigma_1(s-t)} - e^{T(\sigma_2 - 2\sigma_1) + \sigma_2(t-s)}).$$

Therefore we have that $\tilde{a}_2(t)$ is given by:

$$\frac{\xi^2 B_{1,1}^2}{2\sigma_1 - \sigma_2}(1 - e^{T(\sigma_2 - 2\sigma_1)}).$$

Note that T is the integration time of the equations for $\tilde{a}_1$ and $\tilde{a}_2$. So if we want to take the whole history into account we should take the limit for $T \to \infty$.

If $\sigma_2 - 2\sigma_1 < 0$, we have that

$$\lim_{T\to\infty} e^{T(\sigma_2 - 2\sigma_1)} = 0.$$

In this case we obtain:

$$\lim_{T\to\infty} \tilde{a}_2(t) = \frac{\xi^2 B_{1,1}^2}{2\sigma_1 - \sigma_2}.$$

However what if $\sigma_2 - \sigma_1 - \sigma_1 \geq 0$? If $\sigma_2 - 2\sigma_1 = 0$ then the above derivation does not hold, because we divide by $\sigma_2 - 2\sigma_1$.

If $\sigma_2 - 2\sigma_1 > 0$ there are a few options to proceed: If $B_{1,1}^2 = 0$, there is no problem, because then we will simply have $\tilde{a}_2 = 0$. If $B_{1,1}^2 \neq 0$ we have a bigger issue. An option is to still consider the backward-forward system of above, but now use a smaller integration time T for obtaining $\tilde{a}_2(t)$ (we then do not use the analytic expression for h^1, but approximate $\tilde{a}_2$ for each time step numerically). Or one could simply ignore the non-resonance condition and still use $\tilde{a}_2(t) = \frac{\xi^2 B_{1,1}^2}{2\sigma_1 - \sigma_2}$ and see how this works out. The above reasoning explains why we have

the cross non-resonance condition (26).

Note that $\xi = a_1(t)$ and if we define:

$$M_n^{i_1,i_2} = \frac{1}{\sigma_{i_1} + \sigma_{i_2} - \sigma_n},$$

we can rewrite the above as:

$$\lim_{T\to\infty} \tilde{a}_2(t) = B^2_{1,1} M_2^{1,1} a_1(t) * a_1(t),$$

and this is exactly the expression we would get from our parameterising manifold approach. So the above expression is exactly $h^{(1),2}_{\lambda,f}(a_1)$ in the deterministic case with $m = 1$ and $r = 2$.

If we substitute $\tilde{a}_2(t)$ for $a_2(t)$ in the equation for a_1 we obtain:

$$\frac{\partial a_1}{\partial t} = \sigma_1 a_1 + \mathbf{l}_1^H B(a_1 \mathbf{r}_1 + B^2_{1,1} M_2^{1,1} a_1^2 \mathbf{r}_2), \qquad t > 0,$$

and so we keep an expression which only contains $a_1(t)$ and therefore can be (numerically) solved. We obtain:

$$\frac{\partial a_1}{\partial t} = \sigma_1 a_1 + a_1^2 B^1_{1,1} + a_1^3 B^2_{1,1} M_2^{1,1} (B^1_{1,2} + B^1_{2,1}) + a_1^4 \left(B^2_{1,1} M_2^{1,1}\right)^2 B^1_{2,2}, \qquad t > 0.$$

6 PM-based reduced systems: explicit formulas for the deterministic case

In order to describe the resulting "small-scale" parameterisation formulas that we get by application of the parameterising manifold method, we consider again the *nonlinear interaction coefficients* (22):

$$\begin{aligned} B^k_{pq} &= \langle \mathbf{l}_k, B(\mathbf{r}_p, \mathbf{r}_q)\rangle, \ \forall\, p,\ q,\ k \in \mathbb{N}^*, \\ &:= \mathbf{l}_k^H B(\mathbf{r}_p, \mathbf{r}_q). \end{aligned} \tag{32}$$

Note that now k, p, q are not restricted to $\{1, ..., m\}$, but are in $\mathbb{N}^*$. These coefficients describe three types of nonlinear interactions when projected against a given $\mathbf{l}_k$-mode: the self-interactions of the resolved $\mathbf{r}$-modes (when $p, q \in \{1, ..., m\}$), the cross-interactions between the resolved and unresolved $\mathbf{r}$-modes (when $p \in \{1, ..., m\}$ and $q \geq m + 1$, or *vice versa*), and the self-interactions between the unresolved $\mathbf{r}$-modes (when $p, q \geq m + 1$).

We substitute $v_c + v_s$ for v. Now equation (16) gives:

$$\mathcal{M} \frac{\mathrm{d}v_c + v_s}{\mathrm{d}t} \approx \mathcal{J}_{\lambda,f}(v_c + v_s) + B(v_c + v_s, v_c + v_s). \tag{33}$$

For the left hand side of this equation we get:

$$\mathcal{M} \frac{\mathrm{d}v_c + v_s}{\mathrm{d}t} = \mathcal{M} \frac{\mathrm{d}v_c}{\mathrm{d}t} + \mathcal{M} \frac{\mathrm{d}v_s}{\mathrm{d}t} = \mathcal{M}\mathbf{R}_m \frac{\mathrm{d}\mathbf{a}_m}{\mathrm{d}t} + \mathcal{M}\mathbf{R}_{r-m} \frac{\mathrm{d}\mathbf{a}_{r-m}}{\mathrm{d}t}. \tag{34}$$

Preferred is an equation which contains only the first m modes; therefore we multiply by $\mathbf{L}_m^H$. Because of the bi-orthogonal relation equation (17) we get:

$$\mathbf{L}_m^H (\mathcal{M}\mathbf{R}_m \frac{\mathrm{d}\mathbf{a}_m}{\mathrm{d}t} + \mathcal{M}\mathbf{R}_{r-m} \frac{\mathrm{d}\mathbf{a}_{r-m}}{\mathrm{d}t}) = \mathbf{I}_m \frac{\mathrm{d}\mathbf{a}_m}{\mathrm{d}t} = \left(\frac{\mathrm{d}a_1}{\mathrm{d}t}, ..., \frac{\mathrm{d}a_m}{\mathrm{d}t}\right).$$

For the right hand side of equation (33) we get:

$$\mathcal{J}_{\lambda,f}(v_c + v_s) = \mathcal{J}_{\lambda,f}\mathbf{R}_m \mathbf{a}_m + \mathcal{J}_{\lambda,f}\mathbf{R}_{r-m}\mathbf{a}_{r-m}. \tag{35}$$

We multiplied the left hand side of equation (33) with $\mathbf{L}_m^H$, hence we also have to multiply this term by $\mathbf{L}_m^H$. Using equation (17) we see that:

$$\mathbf{L}_m^H(\mathcal{J}_{\lambda,f}\mathbf{R}_m\mathbf{a}_m + \mathcal{J}\mathbf{R}_{r-m}\mathbf{a}_{r-m}) = \mathbf{\Sigma}_m\mathbf{a}_m + 0 = (\sigma_1 a_1, ..., \sigma_m a_m)\,.$$

For the term $B(v_c + v_s, v_c + v_s)$ we obtain:

$$B(v_c + v_s, v_c + v_s) = B(\mathbf{R}_m\mathbf{a}_m + \mathbf{R}_{r-m}\mathbf{a}_{r-m}, \mathbf{R}_m\mathbf{a}_m + \mathbf{R}_{r-m}\mathbf{a}_{r-m}) =$$

$$B(\mathbf{R}_m\mathbf{a}_m, \mathbf{R}_m\mathbf{a}_m) + B(\mathbf{R}_m\mathbf{a}_m, \mathbf{R}_{r-m}\mathbf{a}_{r-m}) + B(\mathbf{R}_{r-m}\mathbf{a}_{r-m}, \mathbf{R}_m\mathbf{a}_m) + B(\mathbf{R}_{r-m}\mathbf{a}_{r-m}, \mathbf{R}_{r-m}\mathbf{a}_{r-m}).$$

We see that if we multiply the above equation by $\mathbf{L}_m^H$ we do not get rid of the terms $a_{m+1}, ..., a_r$. To obtain an ordinary differential equation for the amplitudes $\mathbf{a}_m$ which only depends on $\mathbf{a}_m$, we parameterise $v_s = \mathbf{R}_{r-m}\mathbf{a}_{r-m}$ by the parameterising manifold $h^1(\mathbf{a}_m)$. We obtained in (27) the following formula for our parameterising manifold:

$$h_{\lambda,f}^{(1)}(\xi) = \sum_{n=m+1}^{r} h_{\lambda,f}^{(1),n}(\xi)\mathbf{r}_n, \qquad \forall\ \xi \in \mathcal{H}^{\mathfrak{c}}, \tag{36}$$

where

$$h_{\lambda,f}^{(1),n}(\xi) = \sum_{i_1,i_2=1}^{m} B_{i_1 i_2}^n M_n^{i_1 i_2}\xi_{i_1}\xi_{i_2}, \tag{37}$$

for $m+1 \leq n \leq r$. We have that $h_{\lambda,f}^{(1),n}(\mathbf{a}_m) \approx a_n$.

The $M_n^{i_1 i_2}$ coefficients are given by equation (30). Recall that by nature these coefficients depend on λ and f, since the σ_j are eigenvalues of $\mathcal{J}_{\lambda,f}$. We obtain:

$$B\left(v_c + v_s, v_c + v_s\right) = B\left(v_c + h_{\lambda,f}^1(\mathbf{a}_m), v_c + h_{\lambda,f}^1(\mathbf{a}_m)\right) =$$

$$B\left(\mathbf{R}_m\mathbf{a}_m + \sum_{n=m+1}^{r} h_{\lambda,f}^{(1),n}(\mathbf{a}_m)\mathbf{r}_n, \mathbf{R}_m\mathbf{a}_m + \sum_{n=m+1}^{r} h_{\lambda,f}^{(1),n}(\mathbf{a}_m)\mathbf{r}_n\right).$$

We multiply this equation by $\mathbf{L}_m^H$, we get:

$$\mathbf{L}_m^H\left[B\left(\mathbf{R}_m\mathbf{a}_m + \sum_{n=m+1}^{r} h_{\lambda,f}^{(1),n}(\mathbf{a}_m)\mathbf{r}_n, \mathbf{R}_m\mathbf{a}_m + \sum_{n=m+1}^{r} h_{\lambda,f}^{(1),n}(\mathbf{a}_m)\mathbf{r}_n\right)\right] =$$

$$\left(\mathbf{l}_1^H B\left(\mathbf{R}_m\mathbf{a}_m + \sum_{n=m+1}^{r} h_{\lambda,f}^{(1),n}(\mathbf{a}_m)\mathbf{r}_n\right), ..., \mathbf{l}_m^H B\left(\mathbf{R}_m\mathbf{a}_m + \sum_{n=m+1}^{r} h_{\lambda,f}^{(1),n}(\mathbf{a}_m)\mathbf{r}_n\right)\right).$$

Here we use the notation $B(x) = B(x, x)$ for compactness.

We get the $h^{(1)}$-based reduced system of equation (33), that takes the following compact form:

$$\frac{\mathrm{d}a_j}{\mathrm{d}t} = \sigma_j a_j + \left\langle \mathbf{l}_j, B\Big(\mathbf{R}_m\mathbf{a}_m(t) + \sum_{n=m+1}^{r} h_{\lambda,f}^{(1),n}(\mathbf{a}_m(t))\mathbf{r}_n\Big)\right\rangle,\ 1 \leq j \leq m. \tag{38}$$

We obtain thus for any $j \in \{1, ..., m\}$, that:

$$\begin{aligned}
&\Big\langle \mathbf{l}_j, B\Big(\sum_{i=1}^{m} a_i \mathbf{r}_i + \sum_{n=m+1}^{r} h_{\lambda,f}^{(1),n}(\mathbf{a}_m)\mathbf{r}_n\Big)\Big\rangle \\
&= \sum_{i_1,i_2=1}^{m} a_{i_1}a_{i_2}\langle \mathbf{l}_j, B(\mathbf{r}_{i_1}, \mathbf{r}_{i_2})\rangle \\
&\quad + \sum_{i=1}^{m}\sum_{n=m+1}^{r} a_i h_{\lambda,f}^{(1),n}(\mathbf{a}_m)\Big(\langle \mathbf{l}_j, B(\mathbf{r}_i, \mathbf{r}_n)\rangle + \langle \mathbf{l}_j, B(\mathbf{r}_n, \mathbf{r}_i)\rangle\Big) \\
&\quad + \sum_{n_1,n_2=m+1}^{r} h_{\lambda,f}^{(1),n_1}(\mathbf{a}_m)h_{\lambda,f}^{(1),n_2}(\mathbf{a}_m)\langle \mathbf{l}_j, B(\mathbf{r}_{n_1}, \mathbf{r}_{n_2})\rangle \\
&= \sum_{i_1,i_2=1}^{m} B_{i_1i_2}^{j} a_{i_1}a_{i_2} + \sum_{i=1}^{m}\sum_{n=m+1}^{r} (B_{in}^{j} + B_{ni}^{j}) a_i h_{\lambda,f}^{(1),n}(\mathbf{a}_m) \\
&\quad + \sum_{n_1,n_2=m+1}^{r} B_{n_1n_2}^{j} h_{\lambda,f}^{(1),n_1}(\mathbf{a}_m)h_{\lambda,f}^{(1),n_2}(\mathbf{a}_m).
\end{aligned} \tag{39}$$

Now, using (37) in (39), we find by rearranging the terms:

$$\begin{aligned}
&\Big\langle \mathbf{l}_j, B\Big(\sum_{i=1}^{m} a_i \mathbf{r}_i + \sum_{n=m+1}^{r} h_{\lambda,f}^{(1),n}(\mathbf{a}_m)\mathbf{r}_n\Big)\Big\rangle \\
&= \sum_{i_1,i_2=1}^{m} B_{i_1i_2}^{j} a_{i_1}a_{i_2} + \sum_{i,i_1,i_2=1}^{m}\sum_{n=m+1}^{r} (B_{in}^{j} + B_{ni}^{j}) B_{i_1i_2}^{n} M_n^{i_1i_2} a_{i_1}a_{i_2}a_i \\
&\quad + \sum_{n_1,n_2=m+1}^{r}\sum_{i_1,i_2=1}^{m}\sum_{i_3,i_4=1}^{m} B_{n_1n_2}^{j} B_{i_1i_2}^{n_1} B_{i_3i_4}^{n_2} M_{n_1}^{i_1i_2} M_{n_2}^{i_3i_4} a_{i_1}a_{i_2}a_{i_3}a_{i_4}.
\end{aligned} \tag{40}$$

By substituting (40) in (38), the following $h^{(1)}$-based system of *reduced equations* is obtained as:

$$\begin{aligned}
\mathrm{d}a_j = \Bigg(&\sigma_j a_j + \overbrace{\sum_{i_1,i_2=1}^{m} B_{i_1i_2}^{j} a_{i_1}a_{i_2}}^{(a)} \\
&+ \overbrace{\sum_{i,i_1,i_2=1}^{m}\sum_{n=m+1}^{r} (B_{in}^{j} + B_{ni}^{j}) B_{i_1i_2}^{n} M_n^{i_1i_2} a_{i_1}a_{i_2}a_i}^{(b)} \\
&+ \underbrace{\sum_{n_1,n_2=m+1}^{r}\sum_{i_1,i_2=1}^{m}\sum_{i_3,i_4=1}^{m} B_{n_1n_2}^{j} B_{i_1i_2}^{n_1} B_{i_3i_4}^{n_2} M_{n_1}^{i_1i_2} M_{n_2}^{i_3i_4} a_{i_1}a_{i_2}a_{i_3}a_{i_4}}_{(c)}\Bigg)\,\mathrm{d}t, \qquad 1 \le j \le m,
\end{aligned} \tag{41}$$

where B_{pq}^{l} are defined in (32), and $M_n^{i_1i_2}$ are given in (30). Note that (although without discretisation $r = \infty$) in many situations, only finitely many terms B_{pq}^{r} appearing in (b) and (c) of the above equations (41) are nonzero; see [5, Sect. 3.1].

In the case where infinitely many of such terms would be nonzero, the summation should be truncated for a sufficiently large r in practice. Truncating this sum for $r = q$ means that we consider only the eigenvectors $\mathbf{r}_i$

with $m+1 \leq i \leq q$ as unresolved variables and that we discard the other eigenvectors.

As illustrated in [5, Chaps. 6 and 7] and in [2] for the self-adjoint case, the cubic and quartic terms appearing respectively in (41) (b) and (c), convey cross- and self-interactions between the resolved and unresolved **r**-modes that can turn out to be essential for the derivation of reduced models of good modelling skills. If these terms are neglected we get back the approximation of equation (22). Hence the deterministic parameterising manifold approach may be seen as an extension of the Galerkin methods.

Some comments:

- Probably for a certain λ and f the system (41) provides a better reproduction than system (22) of the "true" dynamics on the resolved variables. Terms (b) and (c) of (41) might in the deterministic case be not important when we are close to a bifurcation, but if we are further away from the bifurcation these terms will be important. In stochastic models we can have large excursions caused by (white) noise, therefore terms (b) and (c) are expected to be important to obtain a good stochastic reduced model.
- The reduced system (41) is complex while the original PDE (11) is real, so the number of modes should always include conjugate pairs in order to properly build-up a reduced system; otherwise spurious oscillations or other numerical artefacts could result.

6.1 The stochastic case

For the stochastic case we have, see equation (23):

$$\mathcal{M}\mathrm{d}v = \big(\mathcal{J}_{\lambda,f}v + B(v,v)\big)\mathrm{d}t + \delta\mathcal{M}v \circ \mathrm{d}W_t. \tag{42}$$

Here W_t denotes a one-dimensional Wiener process, $v \circ \mathrm{d}W_t$ is understood in the Stratonovich sense, and $\delta \geq 0$ quantifies the intensity of that noise term.

We use Stratonovich noise instead of Ito noise, because this gives the best physical representation of the processes which are not resolved, because these processes follow standard calculus.
Note that if $v = 0$ then the right hand side of the SDE is zero, so $\mathrm{d}v$ is zero and v remains zero. Therefore if v reaches 0 it is caught there. We will call 0 a trap for v. Note that if we start a perturbation from a stable stationary state, we will quickly enter zero and stay there forever. Therefore studying a stable stationary state with this model is not interesting.

Therefore we consider the case where we start our perturbation v from an unstable stationary state (for example after a supercritical pitchfork or Hopf bifurcation). We substitute $v = v_c + v_s$ in equation (42). For the noise term we obtain:

$$\delta\mathcal{M}v \circ \mathrm{d}W_t \approx \delta(v_c + v_s) \circ \mathrm{d}W_t = \delta\mathcal{M}(\mathbf{R}_m\mathbf{a_m} + \mathbf{R}_{r-m}\mathbf{a_{r-m}}) \circ \mathrm{d}W_t \tag{43}$$

Multiplying this from the left with $\mathbf{L}_m^H$ and using the bi-orthogonal relation results in:

$$\delta\mathbf{L}_m^H\mathcal{M}(\mathbf{R}_m\mathbf{a_m} + \mathbf{R}_{r-m}\mathbf{a_{r-m}}) \circ \mathrm{d}W_t = \delta\mathbf{a_m} \circ \mathrm{d}W_t \tag{44}$$

Following the derivation above and [5, Chap. 5], reduced systems for Eq. (23) take the same structural form as in (41) where each equation for $1 \leq j \leq m$, is perturbed by $\delta a_j \circ \mathrm{d}W_t$, and the $M_n^{i_1 i_2}$ coefficients are no longer given by Eq. (30), but are obtained from an integration of equation (29) that should be performed simultaneously with the integration of the system (45), for a fixed realisation ω of the noise.

We have that the amplitudes are given by:

$$
\begin{aligned}
\mathrm{d}a_j = \Bigg(& \sigma_j a_j + \overbrace{\sum_{i_1,i_2=1}^{m} B^j_{i_1 i_2} a_{i_1} a_{i_2}}^{(a)} \\
& + \overbrace{\sum_{i,i_1,i_2=1}^{m} \sum_{n=m+1}^{r} (B^j_{in} + B^j_{ni}) B^n_{i_1 i_2} M^{i_1 i_2}_n a_{i_1} a_{i_2} a_i}^{(b)} \\
& + \underbrace{\sum_{n_1,n_2=m+1}^{r} \sum_{i_1,i_2=1}^{m} \sum_{i_3,i_4=1}^{m} B^j_{n_1 n_2} B^{n_1}_{i_1 i_2} B^{n_2}_{i_3 i_4} M^{i_1 i_2}_{n_1} M^{i_3 i_4}_{n_2} a_{i_1} a_{i_2} a_{i_3} a_{i_4}}_{(c)} \Bigg) \mathrm{d}t \\
& + \delta a_j \circ \mathrm{d}W_t, \qquad 1 \le j \le m,
\end{aligned}
\tag{45}
$$

where the M terms are obtained from the integration of the equation below. This integration should be performed simultaneously with the integration of the system above for a fixed realisation ω of the noise.

$$
\mathrm{d}M = \Big(1 - \Big(\sigma_{i_1} + \sigma_{i_2} - \sigma_n\Big) M\Big)\, \mathrm{d}t - \delta M \circ \mathrm{d}W_t. \tag{46}
$$

These random coefficients M convey *exogenous* memory effects resulting from the interactions of the noise with the bilinear term in Eq. (23) (these coefficients depending on the past of the noise). Lemma 5.1 in [5] shows that these terms exhibit an exponential decay of correlations making the corresponding reduced systems genuinely non-Markovian as explained in [5, Chap. 5.3]. These non-Markovian features should not be confused with those discussed in [14]; see also [5, Rmk. 5.6].

6.1.1 Numerical schemes

For integrating (41) we used in the deterministic case (just as for the Galerkin method) a Crank-Nicholson scheme to discretise equation (41) in time and a Newton-Raphson method to solve the resulting set of nonlinear algebraic equations.

For integrating (45) and (46) we use an Euler-Maruyama method. Equation (46) is often a stiff equation. To solve this equation with the Euler-Maruyama method we need an extremely small step size in order to have a numerical stable scheme. The Euler-Maruyama integration seemed to work fine for a few cases with low m and r, but failed because of the stiffness problem for higher m.
To get rid of this problem a semi-implicit numerical scheme of [13, Sect. 12.2] is implemented to integrate equation (46), as advised in [5, Eq. (6.14)]. The scheme is called semi-implicit, because the noise is treated explicitly and the other parts implicitly. This method solved the problem. As a start value we used $M = 0$. The start value of M does not seem to be very important, because M converges very fast to its stationary state.

The Ito form of equation (29) is:

$$
\mathrm{d}M = \Big(1 - \Big(\sigma_{i_1} + \sigma_{i_2} - \sigma_n - \delta^2\Big) M\Big)\, \mathrm{d}t - \delta M \mathrm{d}W_t. \tag{47}
$$

Then the semi-implicit Euler method gives: (this is the deterministic implicit Euler scheme with a noise term added which is treated explicitly)

$$
M_{j+1} = M_j + \Big(1 - \Big(\sigma_{i_1} + \sigma_{i_2} - \sigma_n - \delta^2\Big) M_{j+1}\Big)\, \mathrm{d}t - \delta M_j \mathrm{d}W(j).
$$

Here $dW(j)$ is given by $\sqrt{\mathrm{d}t}\zeta_j$ with ζ_j a random number in the interval $(-1, 1)$.

If we solve this for M_{j+1} then this gives:

$$M_{j+1} = \frac{M_j + \mathrm{d}t - \delta M_j \mathrm{d}W(j)}{1 + (\sigma_{i_1} + \sigma_{i_2} - \sigma_n - \delta^2)\mathrm{d}t}.$$

If $\delta = 0$ and $M_{j+1} = M_j$ we get back $M_j = \frac{1}{\sigma_{i_1}+\sigma_{i_2}-\sigma_n}$, which is the formula for the deterministic case as should be the case. In figure 22 we observe that in the stochastic case the M terms are fluctuating around the deterministic equilibrium of M as expected.

A family of semi-implicit Euler schemes [13, Sect. 12.2] for SDEs is given by:

$$M_{j+1} = M_j + \left[\alpha\left(1 - \left(\sigma_{i_1} + \sigma_{i_2} - \sigma_n - \delta^2\right)M_{j+1}\right) + (1-\alpha)\left(1 - \left(\sigma_{i_1} + \sigma_{i_2} - \sigma_n - \delta^2\right)M_j\right)\right]\mathrm{d}t - \delta M_j \mathrm{d}W(j)$$

Note that we get the above scheme for $\alpha = 1$.

6.2 Rectification term

To obtain the final approximation of our stream function ψ using the PM method, M. D. Chekroun [1] advised to also include a rectification term from the high modes. We assume $\mathcal{H}^s$ is span by the $m+1$-th to q-th eigenvector. The rectification term $R^q(t, x, y)$ is defined as follows:

$$R^q(t, x, y) = h(\mathbf{a}_m(t), x, y) = \sum_{n=m+1}^{q} h^{(1),n}_{\lambda,f}[\mathbf{a}_m(t)]\mathbf{r_n}(x, y),$$

with $a_i(t)$ the amplitude of eigenvector i at time t in the PM approximation. Note that $h^{(1),n}_{\lambda,f}[\mathbf{a}_m(t)] \approx a_n$, hence $R^q \approx v_s$. We have that the approximation v of the PM method is given by:

$$v^{PM}(t) = \sum_{j=1}^{m} a_j(t)\mathbf{r_j}(x, y) + R^q(t, x, y),$$

where the a_j are obtained from system (41), and the approximation of the total solution is ($Re[a]$ is the real part of a):

$$\phi(t) = Re[v^{PM}(t)] + \Phi_{\lambda,f}. \tag{48}$$

6.3 Parameterisation defect

The parameterisation defect is a useful indicator to measure how good the nonlinear interactions are resolved by a parameterising manifold.
The parameterisation defect $Q(T)$ is defined as follows:

$$Q(T) = \frac{\int_0^T ||v_s^q(t, x, y, \omega; v_0) - v_s^{PM}(t, x, y, \omega; v_0)||^2 \mathrm{d}t}{\int_0^T ||v_s^q(t, x, y, \omega; v_0)||^2 \mathrm{d}t}$$

where $||..||$ denotes the Euclidean norm and where v_0 is the start value of the perturbation. (As a start value we took each time the amplitude of the first eigenvector set to 1 and the other amplitudes set to zero.)

v_s^{PM} is given by:

$$v_s^{PM} = h(\mathbf{z}(t, \omega), x, y, \omega)$$

where $\mathbf{z} = (z_1, ..., z_m)$ and z_i is the 'true' amplitude of eigenvector i. With the true amplitude we mean the amplitude we get if we run the total system.

Note: the formula for h is stochastic if we consider the stochastic case. Hence if we speak about the parameterisation defect (PD) we mean the deterministic parameterisation defect and if we speak about the stochastic parameterisation defect (SPD) we mean the parameterisation defect in the case that the noise is nonzero.
v_s^q is given by:

$$v_s^q(t, x, y, \omega) = \sum_{i=m+1}^{q} z_i(t, \omega) r_i(x, y).$$

Note: the $z_i(t)$ depend also on our noise realisation ω, because the z_i depend on the solution of the total system, and the total system is forced by noise.

From [5]: "We note that in the case where the trivial steady state is unstable and a stochastic PM is found, $1 - Q$ will refer to its parameterisation quality in some forthcoming discussions. In particular, the more Q will get close to zero, the better the parameterisation quality will be."

The parameterisation defect $Q(T)$ should be between 0 and 1, if $Q(T)$ is bigger than one, then the parameterising manifold does not perform well and we might get a bad approximation of the amplitudes with the PM method.

7 Introducing the problem

We use a low Reynolds number: this implies that we consider a kind of peanut butter ocean. We do this, because the wind-driven circulation for a low Reynolds number already undergoes a lot of bifurcations and we want to have a simple model to test our methods on. Therefore we consider the pitchfork bifurcation which take place for $R \approx 36.6$. In figure 4 and 5 the bifurcation diagram of our model is shown. The bifurcation diagram is computed with the full model. We use an equidistant 36×36 grid. PSIsw denotes the value of the stream function at grid point $(9, 9)$ which is in the south-west of the basin. In figure 4 PSIsw is plotted versus the Reynolds number. The equilibria on the solid blue line are stable equilibria and the equilibria on the dashed red line are unstable equilibria. On the line between the labelled points (a) and (d) the streamlines are symmetric through the line $y = 0.5$ as can be seen in (a) and (d) of figure 5. It can be seen from (b) and (c) of figure 5 that the two new equilibria which are born from the pitchfork bifurcation possess streamlines which are exactly anti symmetric compared to each other. A similar situation is described in figure 5.16 and 5.17 of [6] and in the paper [9].

We see that (a) and (d) of figure 5 give the stream function we expect to get from the Sverdrup balance, see figure 1. The difference is that in figure 5 a western boundary layer is included. Note that we have two gyres, in the north a subpolar gyre (flowing clockwise) and in the south a subtropical gyre (flowing anti-clockwise).

In figure 5b (figure 5c) we see a weakening (strengthening) of the subpolar gyre or strengthening (weakening) of the subtropical gyre. In figure 11a we have plotted the eigenvector which destabilises the symmetric state at the pitchfork bifurcation.

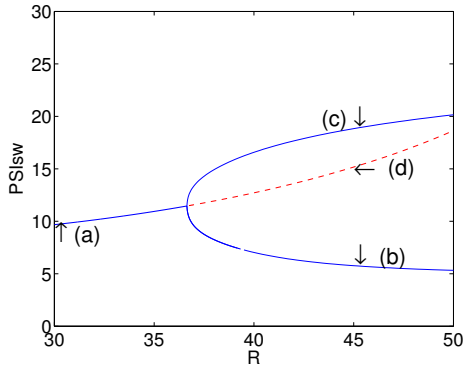

Figure 4: The bifurcation diagram, we see a pitchfork bifurcation at $R \approx 36.65$. In blue the stable branches and in red and dashed the unstable branches. PSIsw is the value of the stream function at grid point $(9, 9)$ in the south west of the basin.

7.1 Parameters

A set of parameter values is chosen. These values are shown in table 1 and are representatives of a basin of 1000×1000 km on a midlatitude β-plane centred around $45°N$. In this paper only the Reynolds number R is used as a bifurcation parameter, the other parameter values will be fixed at their values given in table 1.

The equidistant 36×36 grid was shown to be sufficient to capture all bifurcation points accurately.[9]
Note that the values ρ, τ_0, D and a in table 1 are slightly different from those used in [16].
We use a wind homotopy parameter to switch on the wind. We denote this parameter by W and set $\alpha_\tau = W\frac{\tau_0 L}{\rho D U^2}$. We start with $W = 0$ and when we have found a steady state, we switch on the wind (that is we

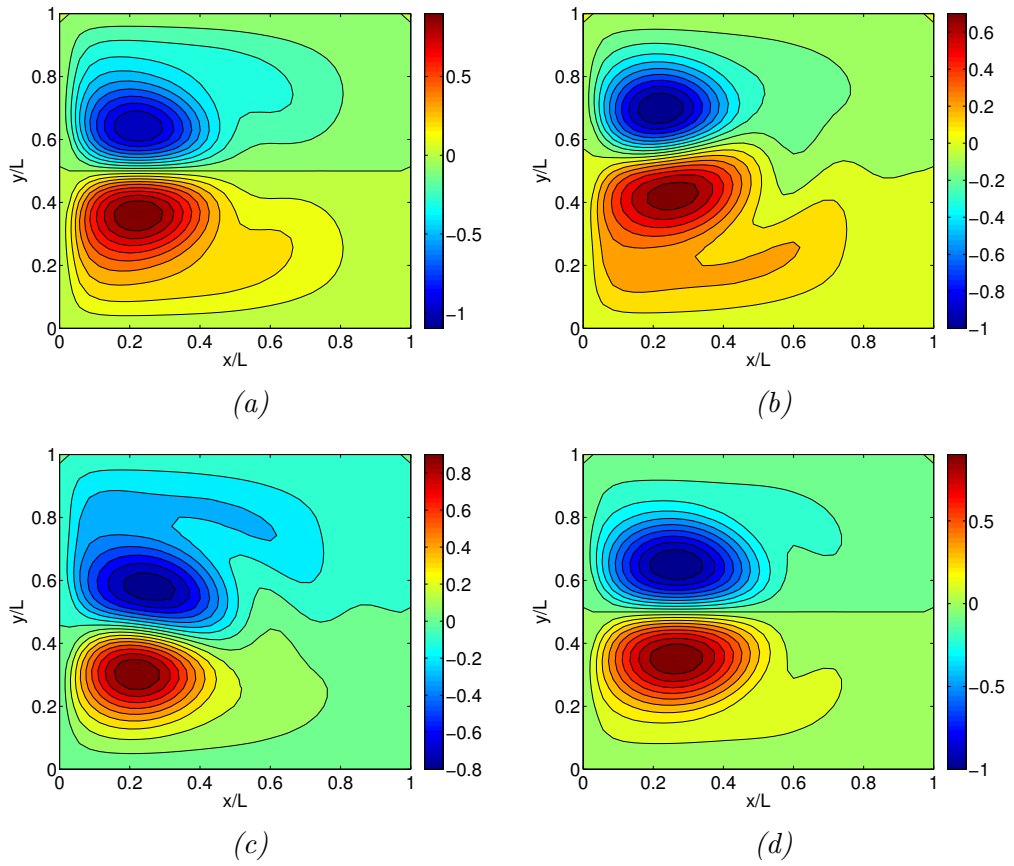

Figure 5: Stationary solutions at labelled points (a)-(d) in Fig. 4. Contour plots are scaled with the absolute maximum and the contour levels are with respect to this maximum. Along the horizontal and vertical axes, the dimensionless quantities x/L and y/L are shown.

Dimensional	Non dimensional
$L = 10^6$ m	$F = 0$
$\beta_0 = 1.6 \times 10^{-11}$ m^{-1} s^{-1}	$A = 1$
$f_0 = 1.0 \times 10^{-4}$ s^{-1}	$\beta = 10^3$
$\rho = 1.026 \times 10^3$ kg m^{-3}	$\alpha_\tau = 10^3$
$\tau_0 = 0.18386$ kg m^{-1} s^{-2}	$a = 0$
$D = 700$ m	
$U = 1.6 \times 10^{-2}$m s^{-1}	

Table 1: Dimensional and nondimensional parameter values.

continue until we have $W = 1$).

Note that the effect of the deformation of the ocean-atmosphere interface is neglected. ($F = 0$).

8 Numerical integration of the SDE

8.1 The full model

Consider the stationary state at the dashed red line for $R = 37$ in figure 4, this is just beyond the pitchfork bifurcation. We denote this stationary state by $\Phi_{\lambda,f}$. At $\Phi_{\lambda,f}$ we calculate all the eigenvalues and all the left and right eigenvectors of $\mathcal{J}_{\lambda,f}$. Note that the eigenvalues of $\mathcal{J}_{\lambda,f}$ determine the stability of our stationary state. We do an initial perturbation $v(0)$ in the direction of the first m right hand eigenvectors $\mathbf{r_i}$. So $v(0) = \sum_{i=1}^{m} \mathbf{r}_i a_j(0)$, with $a_j(t)$ the amplitude of eigenvector j at time t.

This perturbation gives: $\phi(0) = \Phi_{\lambda,f} + v(0)$. Now we let the full model run and we will see that $\phi(t)$ will converge to a stationary state on one of the solid lines of b or c from figure 5, because these are stable equilibria.

With the full model we calculate $\phi(t)$ in time hence $v(t) = \phi(t) - \Phi_{\lambda,f}$ will indicate how the perturbation develops in time. If we know how the perturbation develops in time we can project the perturbation on all the eigenvectors at each time step so that we know how the amplitude of each eigenvector develops in time. We will denote the projection of the perturbation at time t on eigenvector j by $z_j(t)$, so $z_j(t)$ is the 'true' amplitude of eigenvector j at time t.

To calculate the projection of the perturbation on eigenvector j we have to take the inner product of the perturbation at time t with the j-th left eigenvector $\mathbf{l_j}$ and we divide this by the inner product of the j-th left and right eigenvector. This gives:

$$z_j(t) = \frac{< l_j, \phi(t) - \Phi_{\lambda,f} >}{< l_j, r_j >}$$

$z_j(t)$ says how the amplitude of the j-th eigenvector develops in the perturbation v. We will call z_j the 'true' amplitude of the j-th eigenvector of this perturbation at time t.

We examine how well the reduced models approximate the deterministic full model. We therefore ask the following questions:

- Are the 'true' amplitudes of the eigenvectors well approximated?
- Is the stream function well approximated? To answer this question we will compare the true minimum and maximum of the stream function with the approximations and we will plot the true stream function and an approximation
- Is the parameterising manifold able to parameterise the unresolved variables in terms of the resolved variables? To answer this question, we will compute the parameterisation defect.

9 Results

9.1 Deterministic case with Reynolds number 37

We consider the deterministic case, so we set the noise to zero ($\delta = 0$). Consider the unstable dashed red stationary state given in 4 for $R = 37$. We compute the eigenvectors and eigenvalues of $\mathcal{J}_{\lambda,f}$ at this stationary state. In table 2 we see that in this regime there is one eigenvalue bigger than zero, hence we have one unstable eigenvector. In figure 6 how the stream function looks for the unstable symmetric stationary state at $R = 37$.

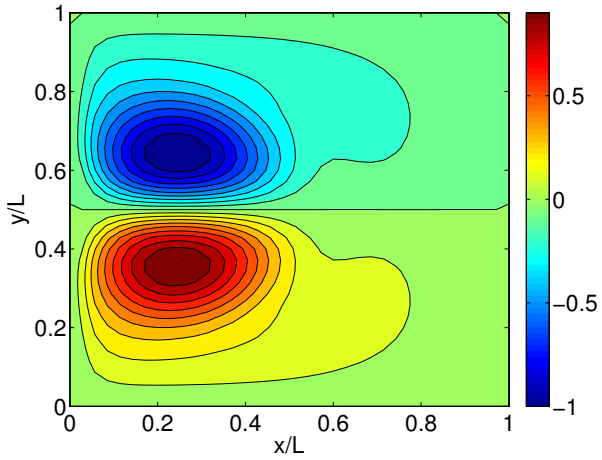

Figure 6: $R = 37$, contour plot of the stream function for the unstable symmetric stationary state $\Phi_{\lambda,f}$

9.2 The perturbation span by one eigenvector

To get an idea how the method works we first consider the case where $\mathcal{H}^c$ is only spanned by the eigenvector with the largest real part. ($\mathcal{H}^c = \alpha \mathbf{r}_1$, $\alpha \in \mathbb{R}$)

Some terminology explained: the eigenvalues are sorted by their real part, so with the first j eigenvectors we denote the j eigenvectors with the biggest real part. Setting $m = k$ means $\mathcal{H}^c$ is spanned by the first k eigenvectors, $q = l$ means $\mathcal{H}^s$ is spanned by the $k+1$-th to l-th eigenvector. By PM we denote that we use the parameterising manifold approach of [5] and by Galerkin we denote that the method of [16] is used.

The true amplitudes of the first four eigenvectors are plotted for $R = 37$ in figure 7. Here the initial perturbation is given by $a_1 = 1$ and $a_i = 0$ for all $i \neq 0$. We will each time start with this perturbation, unless another value is explicitly stated. We observe that if we start with this perturbation we converge to the stable stationary state at the lowest branch of the pitchfork.

9.2.1 Galerkin method

We can apply the deterministic approach of [16]. If $\mathcal{H}^c$ is spanned by 1 eigenvector we obtain from equation (22):

$$\frac{\partial a_1}{\partial t} = \sigma_1 a_1 + B^1_{11} a_1^2$$

Table 2: The first 20 eigenvalues with $R = 37$, Re is the real part of the eigenvalue, Im is the imaginary part of the eigenvalue.

Nr.	Re	Im
1	0.0698	
2	-4.20	
3	-4.31	105
4	-4.31	-105
5	-9.75	-47.1
6	-9.75	47.1
7	-14.2	-73.5
8	-14.2	73.5
9	-14.9	-66.3
10	-14.9	66.3
11	-15.5	
12	-16.6	-37.1
13	-16.6	37.1
14	-21.1	-26.6
15	-21.1	26.6
16	-21.3	-63.1
17	-21.3	63.1
18	-23.6	
19	-24.3	-20.7
20	-24.3	20.7

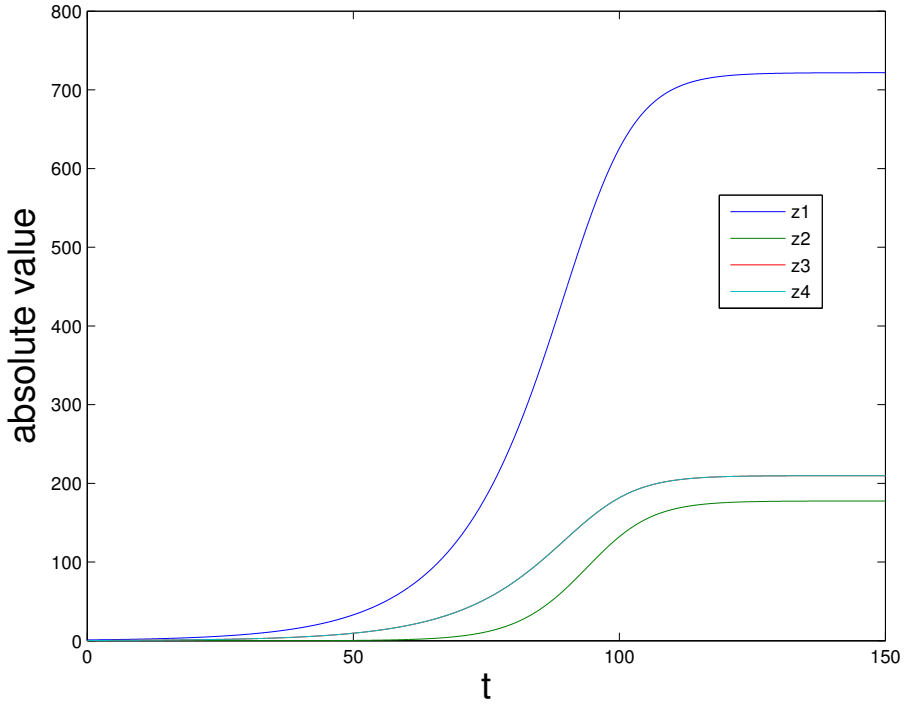

Figure 7: $R = 37$. The 'true' amplitudes z_i of eigenvector i, $z_3 = z_4$ (conjugated pair), z_1 converges to 721.8.

Hence if $\sigma_1 \neq 0$ and $B^1_{11} \neq 0$ we have two equilibria namely $a_1 = 0$ and $a_1 = -\sigma_1/B^1_{11}$. However we have $\sigma_1 = 0.0698464377$ and $B^1_{11} = 0$. If we run the simulation, the solution diverges, because the equilibrium $a_1 = 0$ is unstable and there is no other finite equilibrium for $B^1_{11} = 0$. In figure 8 we plotted the evolution of a_1 in time; one can see that a_1 diverges.

Remark: The Galerkin method is able to give a good approximation of the full model when $\mathcal{H}^c$ is spanned by two eigenvectors. We then have $a_1 \approx 724.5$ and $a_2 \approx 166.6$.

9.2.2 The parameterising manifold approach

System (41) is implemented and we took $m = 1$ and $q = 2$. We saw that in this case a_1 converges to 726.06 after 150 time steps. This is a good approximation of the true amplitude, see figure 7. The minimum and maximum values of the stream function are also well approximated, see table 3.

In figure 9 for $R = 37$ the true solution at the low asymmetric branch is plotted together with the approximation we obtained above for $m = 1$ and $q = 2$. We included more unresolved eigenvectors (so we use a higher q) and plotted the values of the amplitude for $m = 1$ and different q in figure 10. Note that the curves for $q = 2, 4$ and 6 lie all on each other. In table 3 are listed the approximations of the stream function and the parameterisation defect (PD). Observe that the results look reasonable for $q = 2, 4, 6$, but are unreasonable for $q = 8$ and higher. The parameterisation defect is calculated with a time step of 0.05 and 3650 steps, hence the integration time $T = 182.5$.

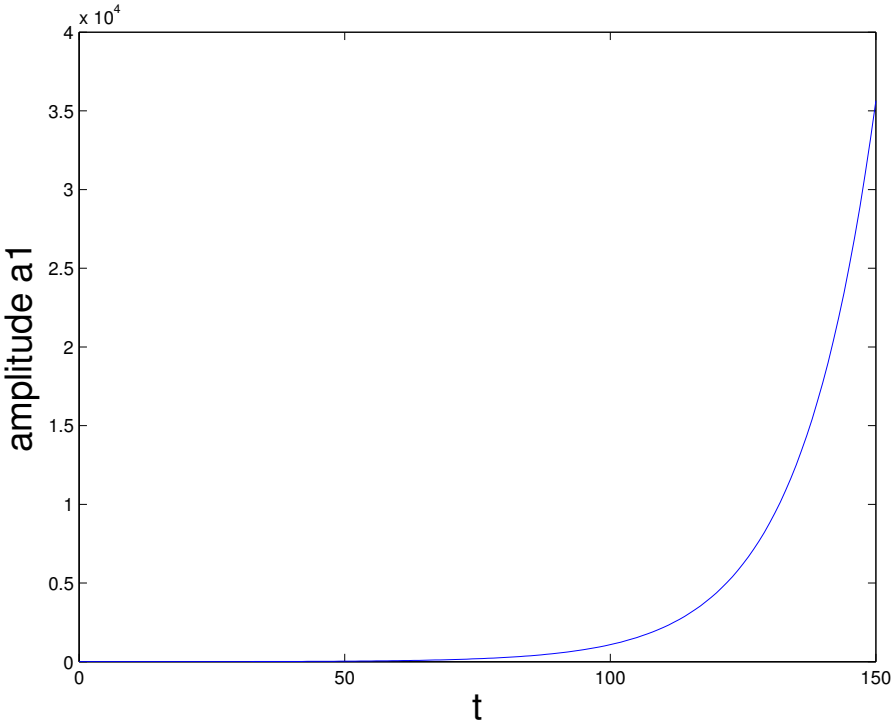

Figure 8: Plot of the amplitude of a_1 in the deterministic model with $\mathcal{H}^c = 1$. We see it diverges.

Observe that from the low value of the parameterisation defect for $q = 2$ we can see that the contribution of the unresolved second eigenvector is well parameterised by the PM in terms of the first eigenvector. If we let $\mathcal{H}^s$ be spanned by 4 and 6 eigenvectors we observe that we still have the same PM, but now there are more unresolved variables to explain, wherefore the PD grows. For $q = 8$ a new PM manifold is constructed, but we see that we obtain a PD above 1. This indicates that the PM 'explains' the unresolved variables poorly and we indeed see that our approximation for $q = 8$ is unreasonable. Note that we do not make reduced models for $q = 3, 5, 7$ et cetera, because the eigenvectors should always be taken in conjugate pairs.

We note the following things about our initial perturbation $v(0) = a_1(0)\mathbf{r}_1$: If we use $a_1(0) = 0$, then a_1 remains zero and we stay at the unstable stationary state. If we use $a_1(0) > 0$ then a_1 converges to a positive value and if we add the approximation of our perturbation to the unstable stationary state we have a good approximation of the stable stationary state at the lower branch of the pitchfork. If we use $a_1(0) < 0$ then a_1 converges to a negative value and with this perturbation we can approximate the stable stationary state at the upper branch of the pitchfork.

The approach of [5] already with $m = 1$ gives good results. However it is strange what happens from $q = 8$ and on.

Because the results from table 3 and figure 10 look strange for $q = 8$ or bigger we investigate this. If $m = 1$ then the right hand side of equation (41) simplifies to an ordinary polynomial of order at most 4 from which we can easily calculate the roots.

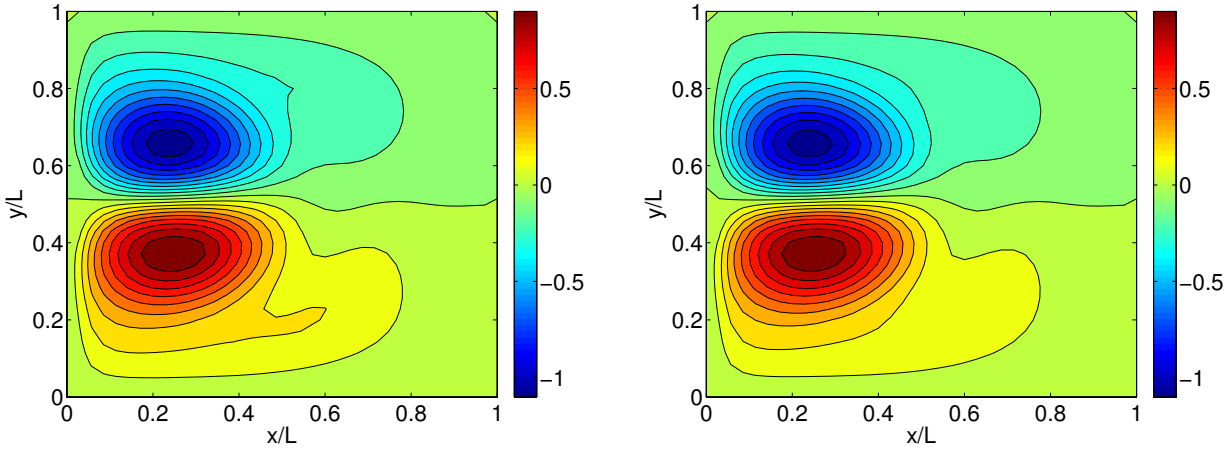

(a) True solution at lower branch *(b) Approx. of the true solution*

Figure 9: For $R = 37$ and $m = 1$ and $q = 2$ we see that the true solution is well approximated.

Table 3: The results of the reduced models with $m = 1$ and $R = 37$

	Psimax	Psimin	Difference max en min	PD
True	21.17	-22.57	-1.400	
Galerkin, m=1	no convergence			
PM, m=1, q=2	20.93	-22.21	-1.282	0.005085
PM, m=1, q=4	”(same)	”	”	0.772
PM, m=1, q=6	”	”	”	0.974
PM, m=1, q=8	no convergence			1.049
PM, m=1, q=10	no convergence			1.002
PM, m=1, q=11	no convergence			1.002
PM, m=1, q=13	no convergence			1.004

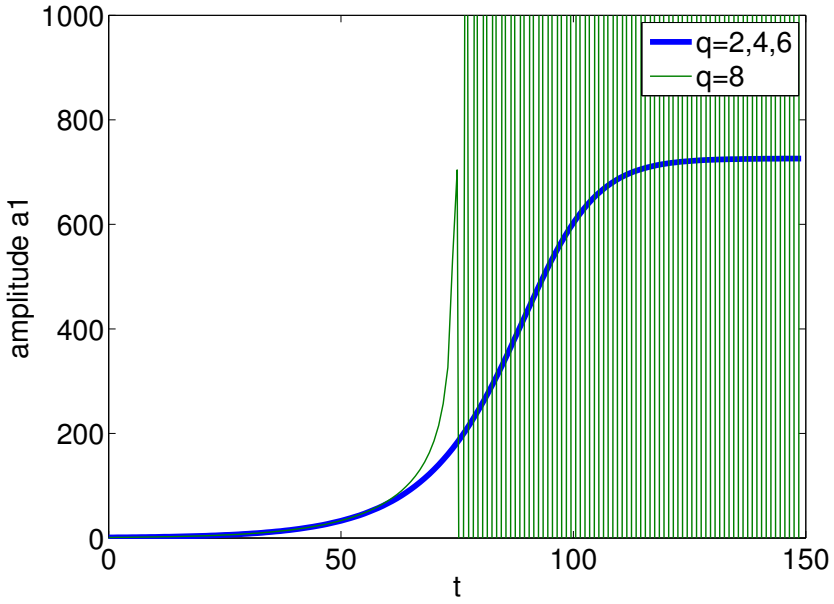

Figure 10: $R = 37, m = 1$. The value of the amplitude for different q. For $q = 2, 4, 6$ $a_1(t)$ converges to 726.1. For $q = 8$ the convergence initially appears good, but then an oscillatory divergence occurs.

For $q = 2$ to 6 we get the same polynomial. We obtain:

$$6.984643776753031 * 10^{-2} a_1 - 1.324948561809644 * 10^{-7} a_1^3.$$

This is the normal form of a supercritical pitchfork. It has three solutions $a_1 = 0$ or $a_1 = \pm 726.06$, of which 0 is an unstable node and the other two are both stable nodes. This are exactly the solutions we have found in figure 10 and from table 3 we know these are quite good approximations, because they lie close to the 'true' amplitude and because the psi max and psi min values were close to the psi max and psi min values of the 'true' solutions.

For $q = 8$ we get the polynomial:

$$6.984643776753031 * 10^{-2} a_1 + 1.893870578237248 * 10^{-6} a_1^3,$$

which has three solutions: $a_1 = 0$ or $a_1 \approx \pm 192.042i$. This is the normal form of a subcritical pitchfork. We have only one real solution $a_1 = 0$ and this solution is unstable, the two complex solutions are stable. Hence if we start with a complex start value we converge to this complex solution. However we started with a real start value and from the simulation we observe that the solutions diverge in an oscillatory manner (if we used start point $a_1 = 1$):

time	Real part	Imaginary part
1.49970E+04	1.44962E+05	-2.15118E-06
1.49980E+04	-1.44967E+05	2.15111E-06
1.49990E+04	1.44972E+05	-2.15104E-06
1.50000E+04	-1.44977E+05	2.15096E-06

For $q = 10, 11$ and 13 and q up to 20 we observe the same problem. The problem is that the coefficient before a_1^3 becomes positive. Consequently we get as solution for a_1 imaginary numbers and we no longer converge to the

right solution. In the above calculations we started each time with a real amplitude, namely $a_1 = 1$. However we could also start with a complex amplitude, in which case we will find the solution $a_1 = \pm 192.042i$ for $q = 8$. The question is what it means that we get a purely imaginary solution for our amplitude.

The first eigenvector is real so if we multiply it by the purely imaginary amplitude we get an imaginary vector and in equation (48) we have to take the real part of this vector (because the original PDE is real) so we get zero. A perturbation of zero is not very interesting, because then we remain in the unstable stationary state $\Phi_{\lambda,f}$.

Another way of looking at this problem is by observing what the eigenvectors look like. In figure 11 the first eight eigenvectors are plotted. Eigenvectors 1 and 2 are real, so only the real part is plotted. For the complex conjugate pairs of eigenvectors only one of the eigenvectors of the pair is plotted.

We observe that $B^j_{1,1}$ is zero for $3 \leq j \leq 6$ (so they do not give a contribution to the polynomial for the evolution of a_1) and that it is nonzero for $q = 2, 7, 8$, and these are exactly the antisymmetric states. If we introduce more resolved eigenvectors or use the Galerkin approach with 8 eigenvectors, these eigenvectors still causes trouble. It might be the case that there is an eigenvector deeper in the spectrum which acts as a rectification term for this eigenvector; such behaviour is also observed in [16].

9.2.3 Computing reduced systems on the fly

If the limit for T to infinity does not exist (for example, because the non-resonance condition is not satisfied) then we might have the case that there is not an analytical expression for the parameterising manifold available. Without an analytical expression for h^1 which gives an approximation of the unresolved variables in terms of the resolved variables, it is still possible to approximate the unresolved variables numerically at each time step by backward-forward systems.

We first implemented such an approach because we did not realize that an analytical expression for the parameterising manifold was available. This numerical procedure associated with the backward-forward system for the PM h^2 is described in [5, Sect. 7.2 and Sect. 7.3] to determine "on the fly" the reduced random vector field. The cornerstone is the pullback characterization of the appropriate stochastic PMs, which allows to update the reduced vector field once $v_c(t; w)$ is known at a particular time instance t.

We implemented system 7.3 of [5]. We constructed the model where $\mathcal{H}^c$ was spanned by the first eigenvector and $\mathcal{H}^s$ was spanned by the second eigenvector and where we used the forward backward integration. This gives figure 12. We see that the amplitude a_1 converges to 726.2, which is close to the true solution of the first amplitude, see figure 7.

However when we tried to do the same with $\mathcal{H}^c$ spanned by 2 eigenvectors, it did not work at first, because we got overflow during the calculations. In equations (7.3c) and (7.3d) of [5] we need to integrate backward, however one of the eigenvalues of $\mathcal{H}^c$ is negative. Hence if we integrate backward (over a too long time) we obtain a huge number. M. D. Chekroun provided us with analytical formulas for the parameterising manifold which solved this issue. Later on we returned to the problem and made the integration time T smaller, which also seemed to solve the problem for $m = 2$ and higher.

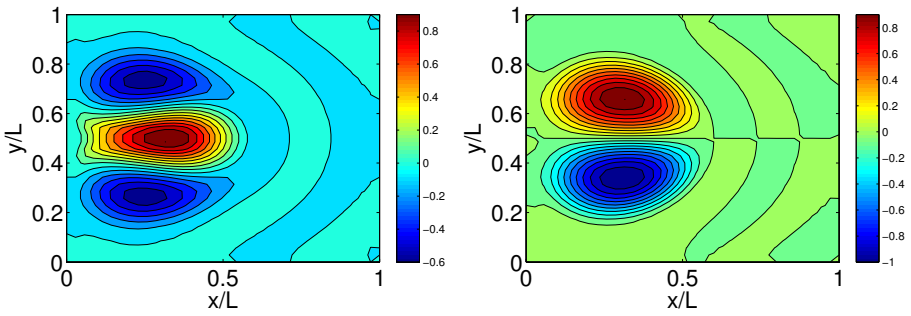

(a) Real part eigenvector 1

(b) Real part eigenvector 2

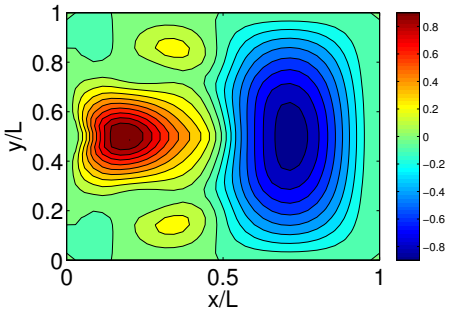

(c) Real part eigenvector 3 and 4

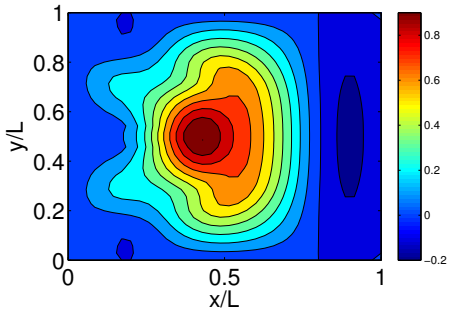

(d) Imaginary part eigenvector 3

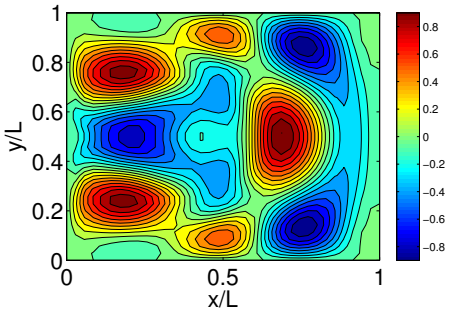

(e) Real part eigenvector 5 and 6

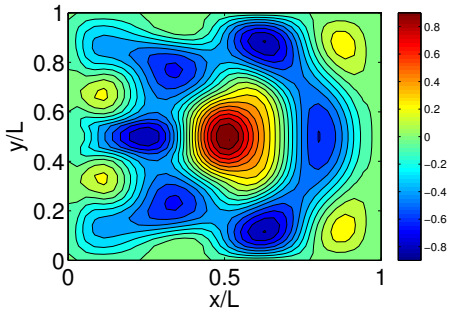

(f) Imaginary part eigenvector 5

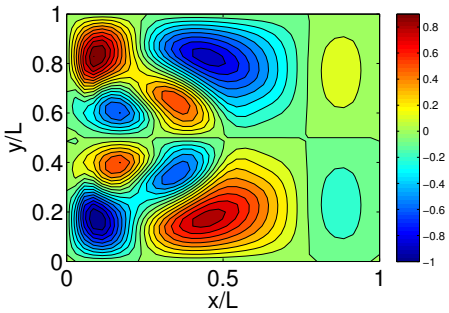

(g) Real part eigenvector 7 and 8

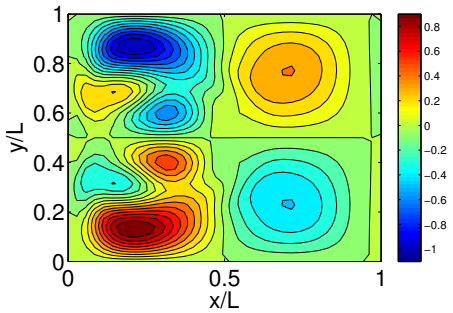

(h) Imaginary part eigenvector 7

Figure 11: The first 8 eigenvectors for $R = 37$. Note that most eigenvectors are reflected through the line $y = 0.5$. Only the second eigenvector and the conjugated pair of eigenvectors 7 and 8 are antisymmetric and these are also the only eigenvectors which contribute to the polynomial.

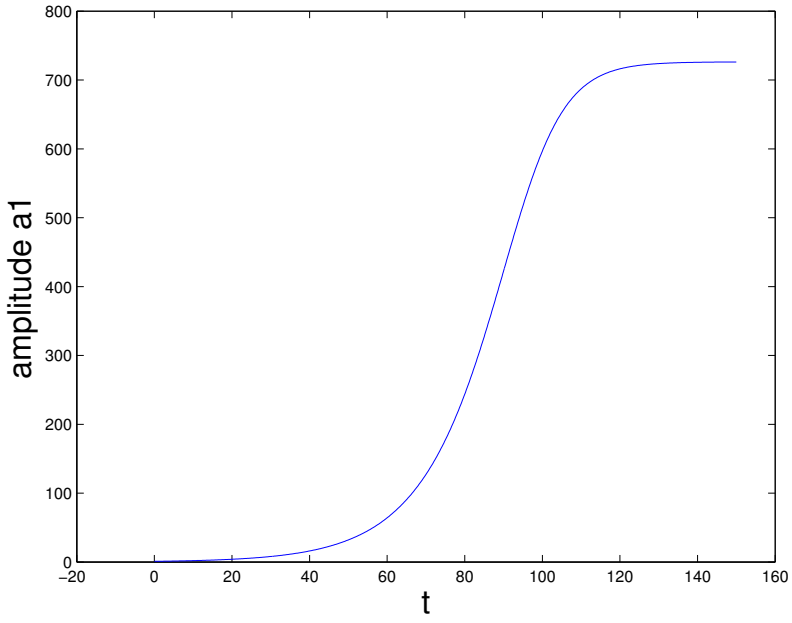

Figure 12: Plot of a_1 obtained by computing v_c "on the fly". a_1 converges to 726.2.

Table 4: The first 20 eigenvalues with $R = 40$.

Nr.	Re	Im
1	0.581	
2	-3.48	
3	-3.61	-105
4	-3.61	105
5	-9.37	47.4
6	-9.37	-47.4
7	-13.5	-66.1
8	-13.5	66.1
9	-13.7	
10	-16.1	-74.8
11	-16.1	74.8
12	-16.7	-37.2
13	-16.7	37.2
14	-19.1	-63.5
15	-19.1	63.5
16	-20.6	27.0
17	-20.6	-27.0
18	-21.6	
19	-23.6	-94.5
20	-23.6	94.5

10 Reynolds number 40

Here we consider the case where we start our perturbation v from the unstable stationary state at $R = 40$. This stationary state is further away from our bifurcation, therefore a reduced model which captures the behaviour of our perturbation v is harder to make. We compute the eigenvalues, this gives table 4. In figure 13 we plotted the true amplitudes of the first six eigenvectors.

For $m = 1$ and $q = 2$ we obtain:

$$\frac{\partial a_1}{\partial t} = 0.58147a_1 - 8.9366 * 10^{-8}a_1^3$$

Solving for the stationary states gives the unstable stationary state: $a_1 = 0$ and the two stable stationary states $a_1 = \pm 2550.81$. In figure 14 we plot the amplitude of a_1 for $m = 1$ and different q. Note that the amplitude a_1 is the same for $q = 2, 4, 6, 8$.

We used for the calculation of the parameterising defect for $R = 40$ a time step of 0.001 and 150 thousand steps, so an integration time $T = 150$. In table 5 we list the approximations of minima and maxima of the stream function and the parameterisation defect for $m = 1$ and different q. Note that the approximations for $q = 2, 4, 6, 8$ are the same. With 'Start' we denote the minimum and maximum values of the stream function from the unstable symmetric stationary state we started from. For $q = 11, 13, 18$ we have the same problem as encountered with $R = 37$ and $(m, q) = (1, 8)$.

Note that the approximation of $m = 1$ and $q = 2$ is already quite good. The parameterisation defect is low (this means that the parameterising manifold with $m = 1$ and $q = 2$ is well able to parameterise with the first

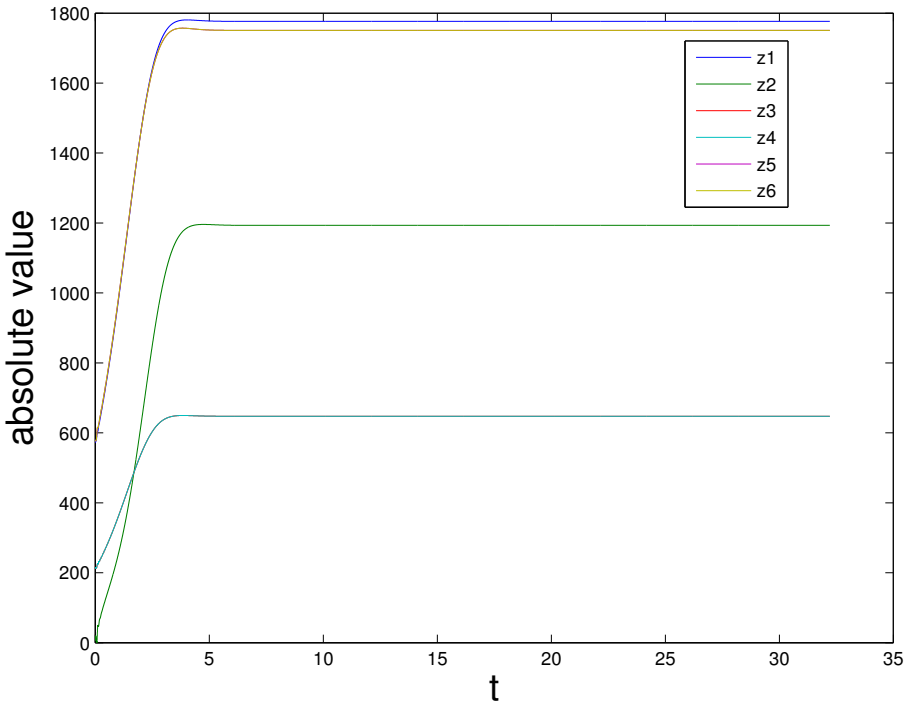

Figure 13: $R = 40$. The true amplitudes z_i of eigenvector i, $z_3 = z_4$ and $z_5 = z_6$ (both are conjugate pairs), z_1 converges to 1776.6

eigenvector the true amplitude times $\mathbf{r}_2$). If we add more eigenvectors our parameterising manifold remains the same, while there are now more resolved eigenvectors to explain, therefore the PD gets higher and higher for $q = 4, 6, 8$. For $q = 9$ a new parameterising manifold is made, but the parameterising manifold now is only able to explain 1.52% of the unresolved eigenvectors. However it is remarkable that we already obtain a good approximation of the true stream function with a perturbation in only one eigenvector.

In table 6 we list the approximations of minima and maxima of the stream function and the parameterisation defect for $m = 2$ and different q. In figure 16 we plot the amplitudes of the reduced models and in figure 17 the approximations of the stream function. For $m = 2$ and $q = 6$ the approximation is quite good.

Table 5: The results of the reduced models with $R = 40$ and $m = 1$.

	Psimax	Psimin	Difference max en min	PD
Start	24.36	-24.36	0	
True'	19.68	-23.38	-3.7	
Galerkin	no conv.			
PM, q=2	19.29	-19.53	-0.24	0.1157
PM, q=4	”			0.4772
PM, q=6	”			0.8553
PM, q=8	”			0.9875
PM, q=9	21.65	-18.20	3.446	0.9848
PM, q=11	no conv.			
PM, q=13	no conv.			
PM, q=18	no conv.			

Table 6: The results of the reduced models with $R = 40$ and $m = 2$.

	Psimax	Psimin	Difference max en min	PD
Start	24.36	-24.36	0	
True'	19.68	-23.38	-3.7	
Galerkin	19.16	-19.42	-0.2673	
PM, q=4	19.02	-19.93	-0.9029	1.040
PM, q=6	19.62	-21.06	-1.445	0.883
PM, q=8	28.14	-31.62	-3.484	0.9134
PM, q=9	25.81	-29.72	-3.910	
PM, q=11	no conv.			
PM, q=13	no conv.			

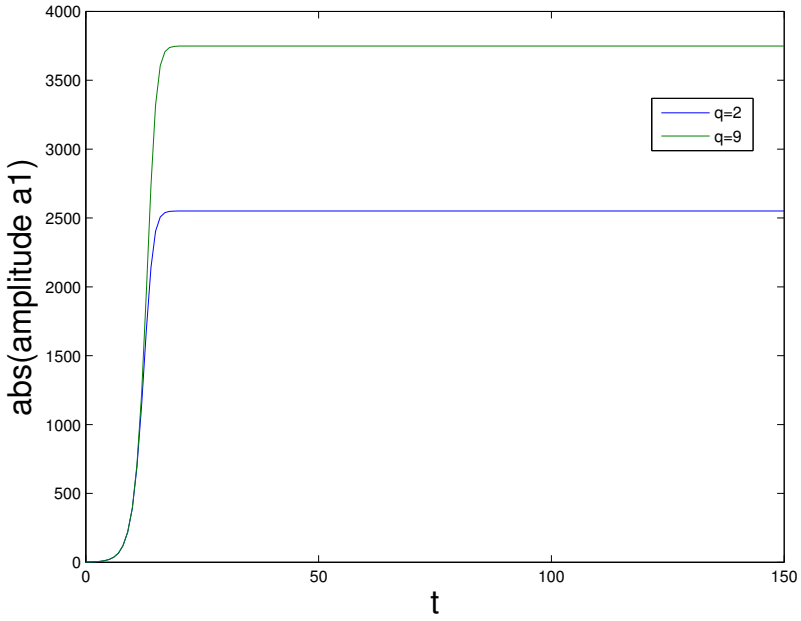

Figure 14: $R = 40$ and $m = 1$.

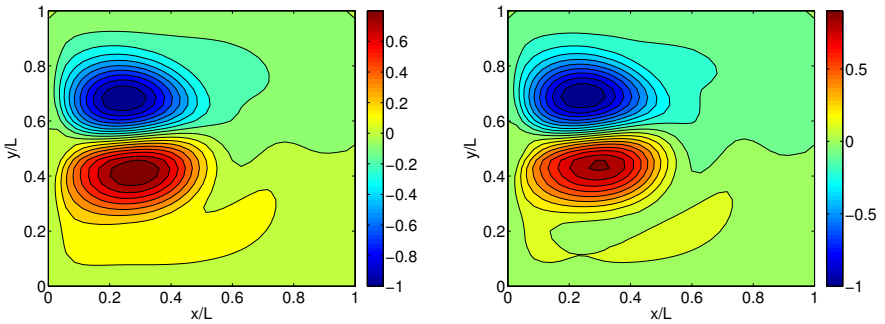

(a) $m = 1$ and $q = 2, 4, 6, 8$ *(b) $m = 1$ and $q = 9$*

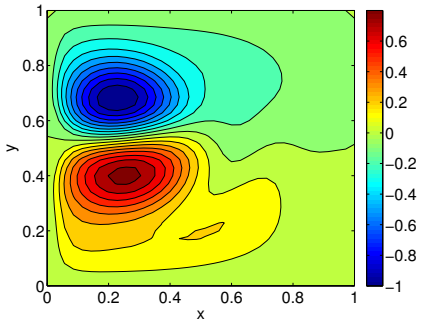

(c) True solution

Figure 15: The true solution and approximations with $m = 1$ for $R = 40$.

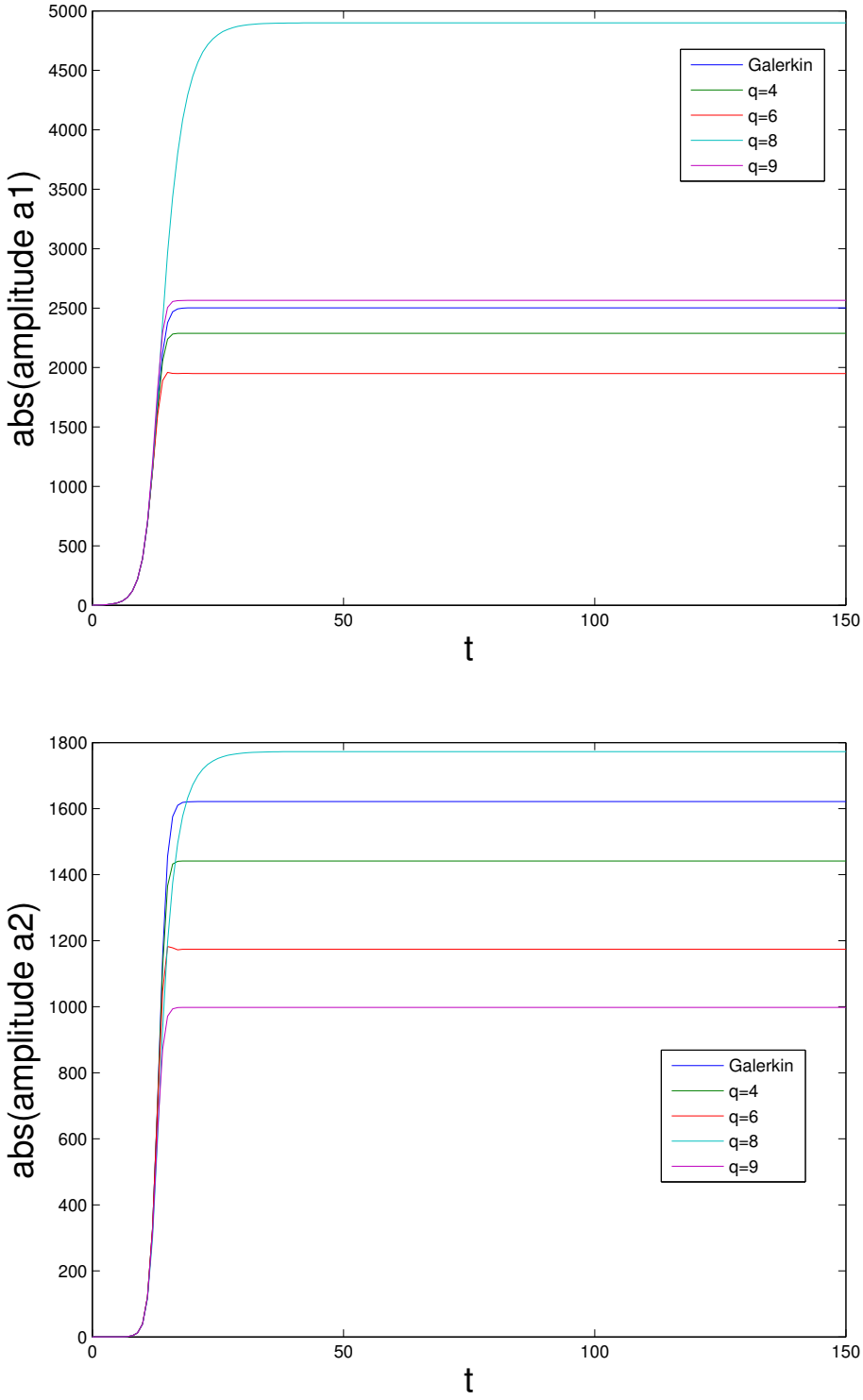

Figure 16: $R = 40$, $m = 2$.

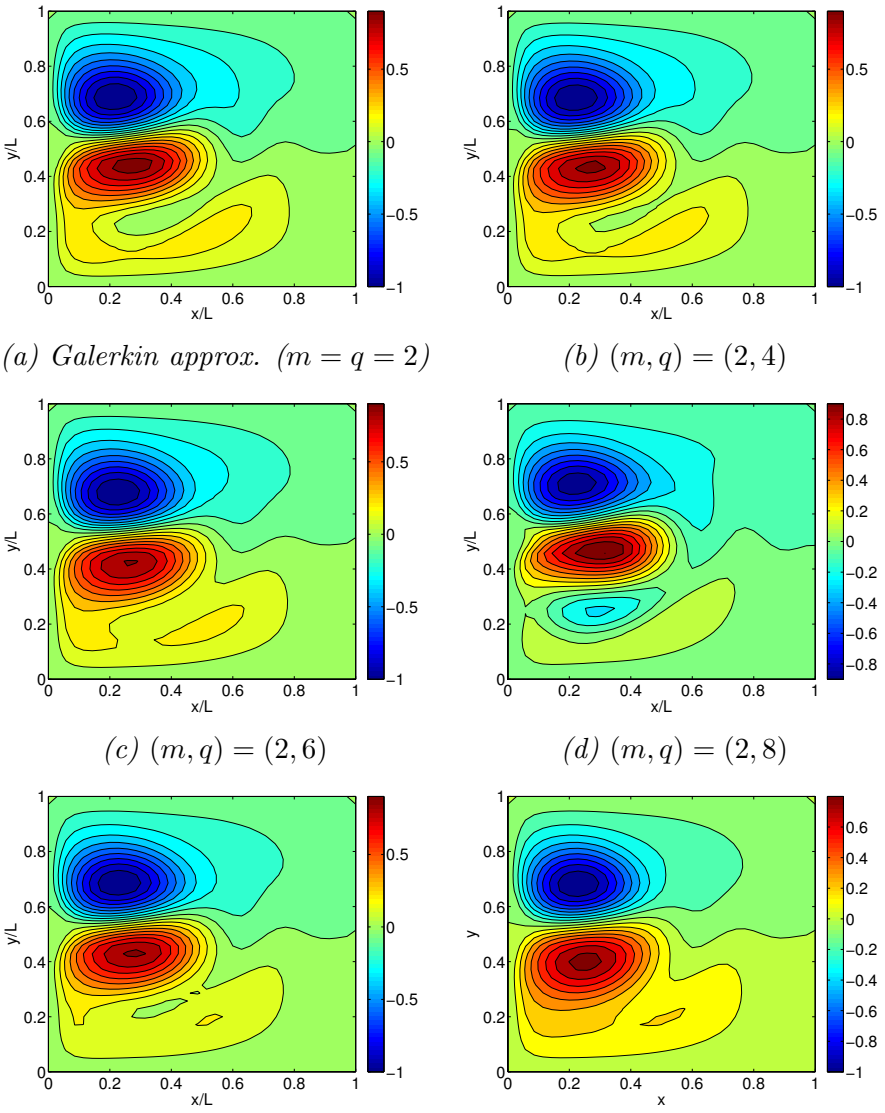

(a) Galerkin approx. ($m = q = 2$) *(b) $(m, q) = (2, 4)$*

(c) $(m, q) = (2, 6)$ *(d) $(m, q) = (2, 8)$*

(e) $(m, q) = (2, 9)$ *(f) True solution*

Figure 17: The true solution and approximations with $m = 2$ for $R = 40$.

11 The stochastic case

We now consider the equation with noise:

$$\mathcal{M}\mathrm{d}v = \big[\mathcal{J}_{\lambda,f}v + B(v,v)\big]\mathrm{d}t + \delta\mathcal{M}v \circ \mathrm{d}W_t.$$

Note that if $v = 0$, then $\mathcal{J}_{\lambda,f}v + B(v,v) = 0$ and $\delta\mathcal{M}v \circ \mathrm{d}W_t = 0$ and therefore v remains zero. We therefore call 0 a trap for v.

11.1 The Fokker-Planck equation

Consider the case with $R = 37$. We consider system (45) with $m = 1$ and $r = 2$ to obtain: (we do not have second and fourth order terms, because $B^1_{1,1} = 0 = B^1_{2,2}$)

$$\mathrm{d}a_1 = \sigma a_1 + (B^1_{1,2} + B^1_{2,1})B^2_{1,1}M_2^{1,1}a_1^3 + \delta a_1 \circ \mathrm{d}W_t, \tag{49}$$

with $M_2^{1,1}$ given by:

$$\mathrm{d}M_2^{1,1} = (1 - (2\sigma_1 - \sigma_2)M_2^{1,1})\mathrm{d}t - \delta M_2^{1,1} \circ \mathrm{d}W_t.$$

Note that the stationary state of $M_2^{1,1}$ in the deterministic case is 0.230642 and that in the deterministic case $(B^1_{1,2} + B^1_{2,1})B^2_{1,1}M_2^{1,1} \approx -1.3249 * 10^{-7}$. Note that 0 is a trap for a_1. We want to set up the Fokker-Planck equation for this SDE, however the problem is that the coefficients before the third and fourth degree terms (the terms involving M) depend on the noise.

To avert this problem we take for these terms the deterministic coefficients. This gives the following polynomial for $R = 37$, $m = 1$ and $q = 2$, which approximates well equation (41) for $m = 1$ and $q = 2$:

$$\mathrm{d}a_1 = (0.069846a_1 - 1.3249 * 10^{-7}a_1^3)\mathrm{d}t + \delta a_1 \circ \mathrm{d}W_t.$$

This case is known in the literature as the stochastic pitchfork with multiplicative noise. This case is also worked out in [8, Sect. 4.3.1]. In the following we set $x = a_1$, $\sigma_1 = 0.069846$, $q_2 = 1.3249 * 10^{-7}$.

We consider the Ito form of the equation above, which is given by:

$$\mathrm{d}a_1 = [(\sigma_1 + \delta^2)a_1 - q_2a_1^3]\mathrm{d}t + \delta a_1 \mathrm{d}W_t.$$

For this equation we have that the forward Fokker-Planck equation gives:

$$\frac{\partial p}{\partial t} + \frac{\partial((\sigma_1 + d^2)x - q_2x^3)p}{\partial x} - \frac{\delta^2}{2}\frac{\partial^2(px^2)}{\partial x^2} = 0$$

with $p(x,t)$ the probability density function. We set $\frac{\partial p}{\partial t} = 0$, because we want to know the stationary distribution of p. Following the derivation of [8, Sect. 4.3.1] we obtain for $x > 0$:

$$p^+(x) = c_1 x^{-(\delta^2 - 2\sigma_1)/\delta^2} e^{-q_2/\delta^2 x^2}.$$

We obtain for $x < 0$:

$$p^-(x) = c_1 (-x)^{-(\delta^2 - 2\sigma_1)/\delta^2} e^{-q_2/\delta^2 x^2}.$$

The values for σ_1 and q_2 are given, but the value of $\delta > 0$ still may be chosen, hence we distinguish a few situations. If $\delta^2 - 2\sigma_1 > 0$ then $p^{\pm}(x)$ is of the form:

$$p^{\pm}(x) = c_1 \frac{e^{-a_2x^2}}{(\pm x)^{a_1}}$$

with constant values $a_i > 0$. Note that in this case $p^{\pm}(x)$ cannot be normalised on $(0, \pm\infty)$. We have:

$$\lim_{x \downarrow 0} p^{+}(x) = \infty,$$

$$\lim_{x \uparrow 0} p^{-}(x) = \infty.$$

Therefore we see that the probability to reach 0 is infinite, while the probability to reach another number is finite. So our probability density function in this case is simply the Dirac delta function.
One can see that if the noise is large enough, $(\delta > \sqrt{2\sigma_1})$, jumping across zero between the two stable stationary states is possible, and that the probability of eventually reaching 0 (and staying there) is 1.

If $\delta^2 - 2\sigma_1 < 0$ then $p^{\pm}(x)$ is of the form:

$$p^{\pm}(x) = c_1(\pm x)^{a_1} e^{-a_2 x^2}$$

with the constant values $a_i > 0$. Note that $p^{\pm}(x)$ can be normalised at $(0, \pm\infty)$ and that the chance to reach 0 is zero. Therefore if the noise is small enough, $\delta < \sqrt{2\sigma_1}$, and we start with either a positive (negative) initial perturbation, then the perturbation remains positive (negative), because the noise on the perturbation is not large enough to enable the perturbed solution to cross zero. We normalised $p^{+}(x)$ and made a plot of $p^{+}(x)$ with $\delta = 0.1$, this gives figure 18.

Letting $\delta = \sqrt{2\sigma_1}$ gives $\delta \approx 0.373755$. Hence the interesting case to study the above system is for a $\delta < 0.373755$, because otherwise the probability density function is simply a Dirac delta function. Our system is quite like the above system and therefore we use $\delta = 0.1$ as amplitude for our noise.

We observe that if we decrease the noise the peak concentrates more around the deterministic stable stationary state and gets more peaked. If we increase the noise we observe that the peak gets broade,r and we observe that the peak moves away from the deterministic stable stationary state to zero until the noise passes the value 0.373755 and we obtain an Dirac delta function. See for examples figures 18 and 19.

Note that that the equation with $(m, q) = (1, 2)$ for $R = 37$ is similar to that for $R = 40$. Therefore in the same way as above we then find that for this equation with $R = 40$ the interesting case is for $\delta < \sqrt{2\sigma_1}$, which in this case gives that $\delta < 1.0784$. Hence we see that (as expected) we need for $R = 40$ greater noise to jump from one stable stationary state to another stable stationary state.

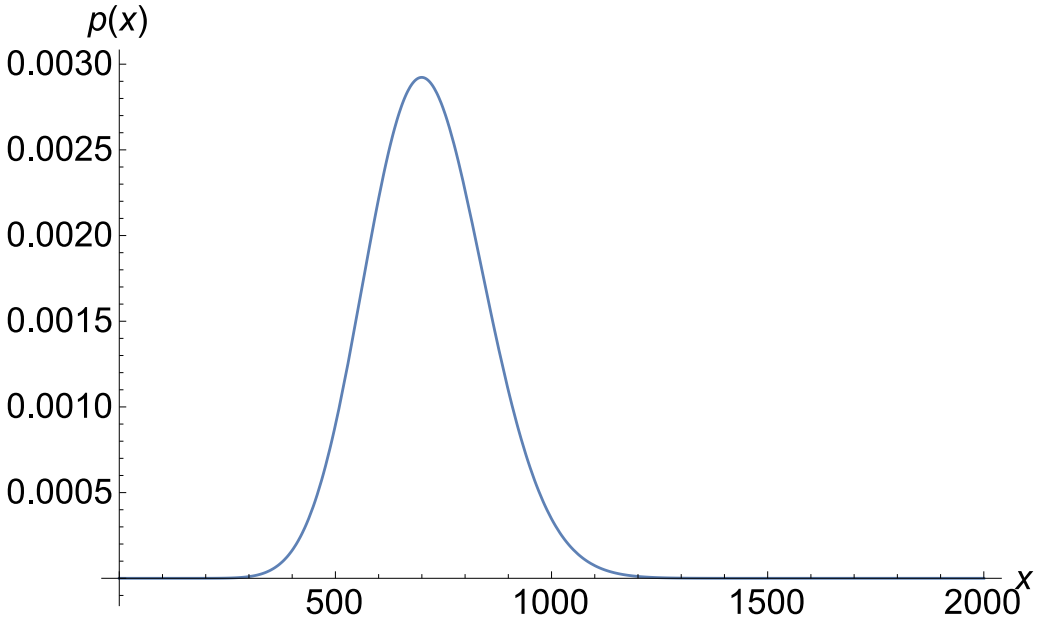

Figure 18: $R = 37$ *and* $\delta = 0.1$. $p^{+}(x)$ *for* $m = 1$ *and* $q = 2$.

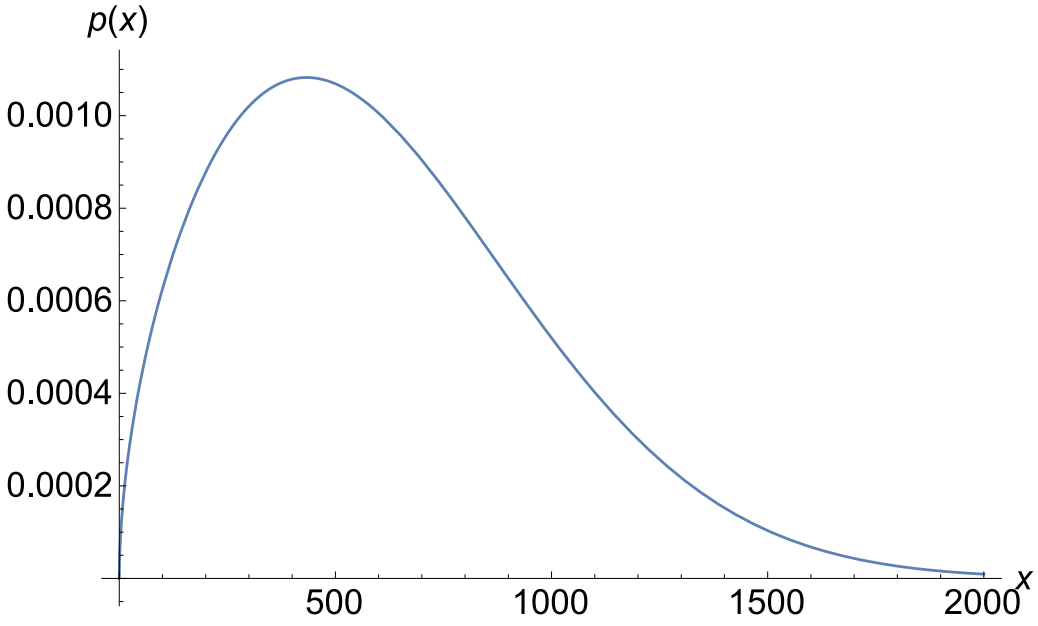

Figure 19: $R = 37$ *and* $\delta = 0.3$. $p^{+}(x)$ *for* $m = 1$ *and* $q = 2$.

11.2 Implementation stochastic term

In the simulations we checked that the non-resonance condition was satisfied. To implement the stochastic reduced system we use $M = 0$ as a start value for equation 29 and we use $a_1 = 1$ and $a_i = 0$ for $i \neq 0$ as the start value for the perturbations. We first consider the system (45) with $R = 37$ and $(m, q) = (1, 2)$.

In figure 20 we display a picture of a_1 with $\delta = 0.1$ and multiplicative noise, we took step size 0.05 and 150.000 steps. The red line is the average. On the x-axis are the number of points, on the y-axis the value of the amplitude. Observe that there is no jumping between the two stable stationary states.

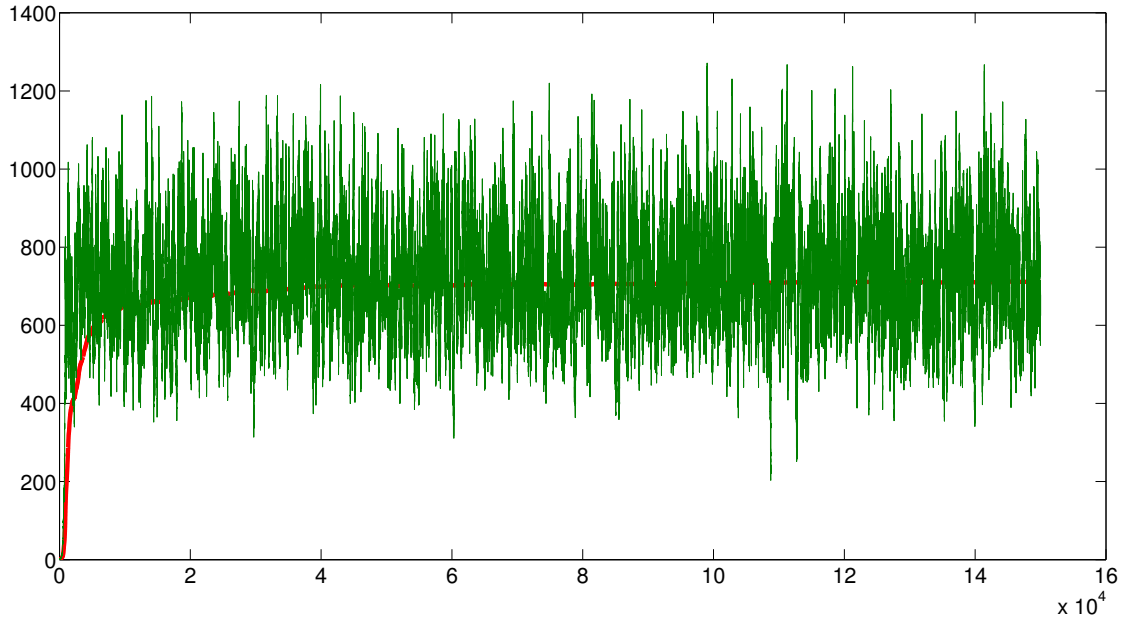

Figure 20: $R = 37$, $m = 1, q = 2$, $\delta = 0.1$, the red line is the average. The average at the end is: 711.08.

To make a probability density function for equation (49) we let the simulation for a_1 run for a long time, and make a histogram. By normalising the histogram we approximate the probability density function.

We use multiplicative noise, $\delta = 0.1$, 15 million time steps and a time step of 0.1. We start with a perturbation $a_1(0) > 0$ and use 1000 bins of the same width, to obtain the PDF of figure 21. Note the resemblance to figure 18. We denote the PDF for all initial perturbations $a_1(0) > 0$ by p^+.

If we start with $a_1(0) = 0$ (without perturbation) we stay at 0 forever, because we use multiplicative noise. Hence this PDF p^0 looks like a Dirac delta function. If we start with a perturbation $a_1(0) < 0$ we get the PDF p^- of figure 23.

In figure 22 $M_2^{1,1}$ is plotted. In the deterministic case we have that $M_2^{1,1} = 1/(\sigma_1 + \sigma_1 - \sigma_1) = 0.230642$. We see that the average of the model with noise is almost the same as this number, as expected.

Figure 24 is made with a time step of 0.1 and 1.5 million steps. Note the resemblance to figure 19, which is made with the M terms given by their stochastic value.

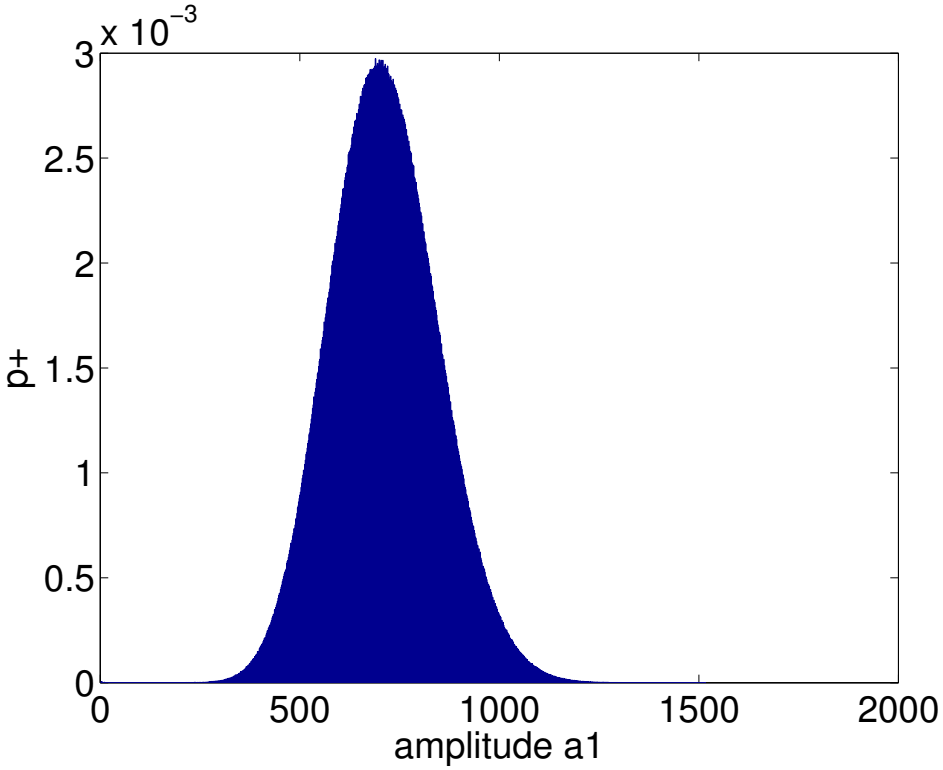

Figure 21: $R = 37$, $\delta = 0.1$. *The probability density function* p^+ *for* $m = 1$ *and* $q = 2$ *and an initial perturbation* $a_1(0) > 0$. *The average is* 710.7927.

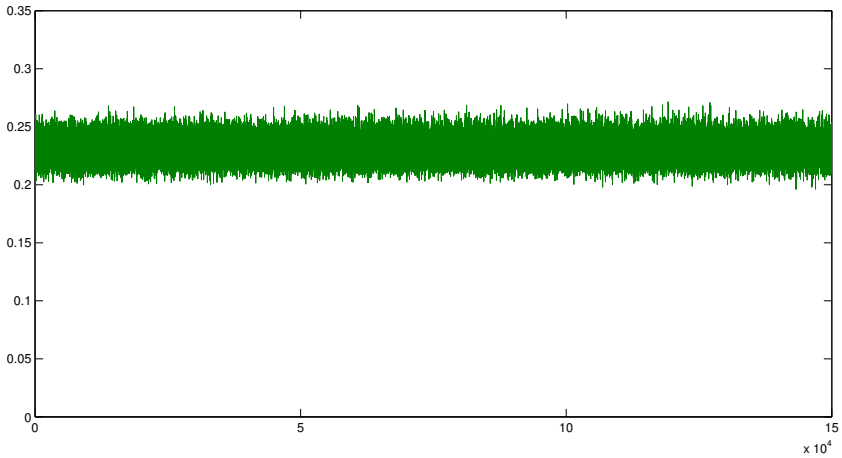

Figure 22: $R = 37$ *and* $\delta = 0.1$. *Generation of* $M_2^{1,1}$ *with noise, 150000 steps, time step is 0.1* $m = 1$ *and* $q = 2$. *The overall average is 0.2309.*

For the model with $m = 2$ we have that a_2 always converges to the same value if $a_1(0) \neq 0$, however a_1 converges to a negative value if $a_1(0) < 0$ and vice versa. Therefore the value of a_1 also determines to which

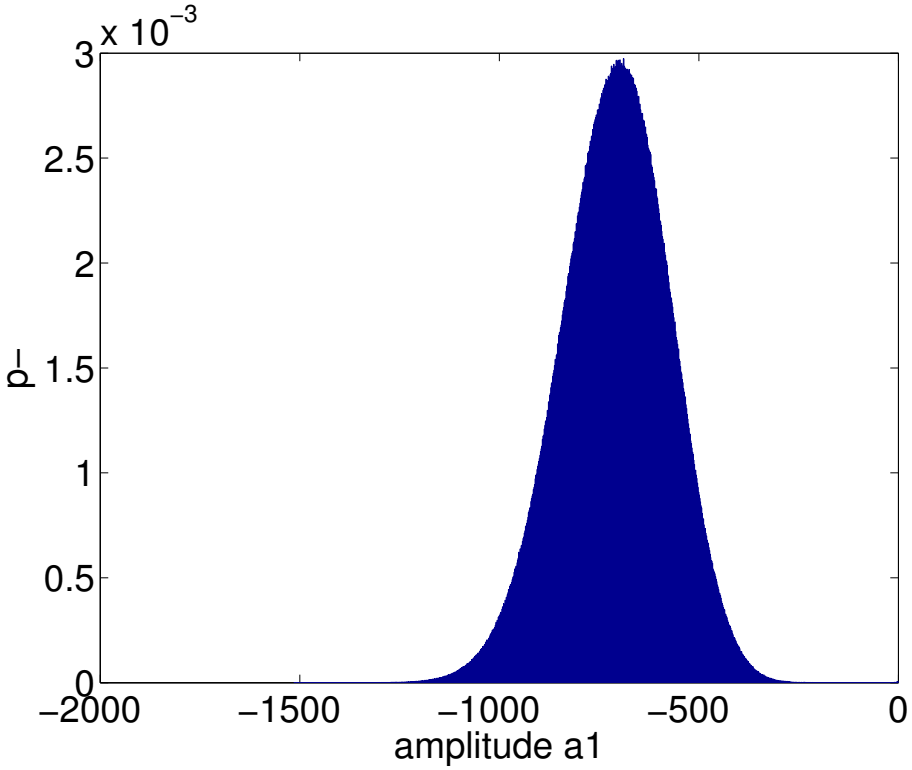

Figure 23: $R = 37$, $\delta = 0.1$. *The probability density function* p^- *for* $m = 1$ *and* $q = 2$ *and an initial perturbation* $a_1(0) < 0$. *The average is* -710.7927.

stable state we converge in the case with $m = 2$, so the value of a_1 is in this case still interesting to plot for obtaining a PDF. In figure 25 we made a PDF p^- for $R = 40$ where the reduced model is given by $(m, q) = (2, 6)$.

The reduced model captures important features of the full model, namely 0 is a trap for the full model and for the reduced model. With the full model one would also expect that (starting with a nonzero perturbation) if the amplitude of the noise δ passes a certain threshold that then the perturbation is able to cross (and therefore also to reach) 0, and that therefore the PDF will look like a Dirac delta function. Object for further study can be what this threshold is.

If one wants to see jumping between the stable stationary states we would suggest to incorporate additive noise (noise in the wind forcing). For additive noise on the full model there are also equations to get a reduced stochastic model based on parameterising manifolds, see [3]. However we did not have the time to include those. This may be a nice idea for further research.

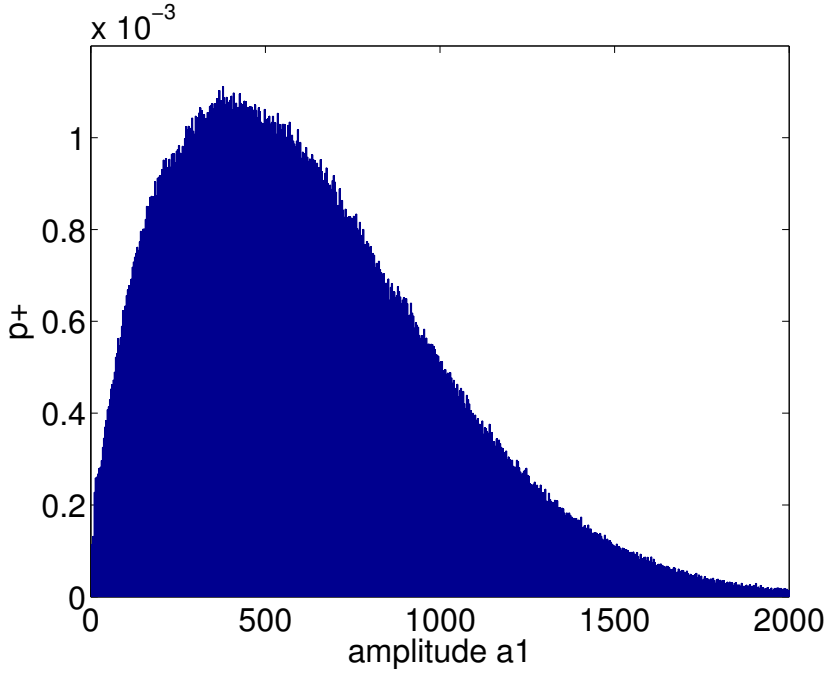

Figure 24: $R = 37$, $\delta = 0.3$. *The probability density function* p^+ *for* $m = 1$ *and* $q = 2$ *and an initial perturbation* $a_1(0) > 0$, *the average is: 626.9.*

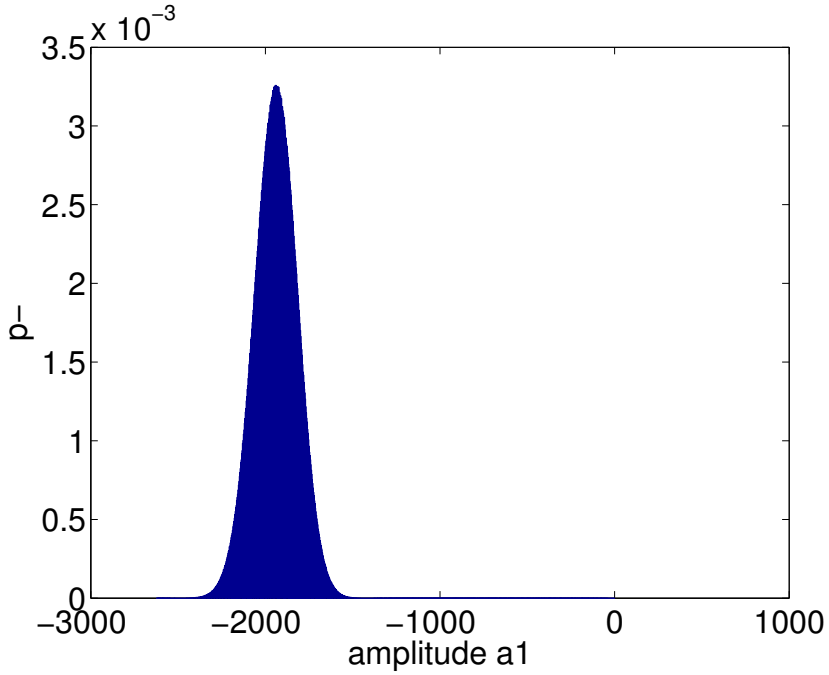

Figure 25: $R = 40$. *The probability density function* p^- *for* $m = 2$ *and* $q = 6$ *and an initial perturbation* $a_1(0) < 0$. *The average is* -1941.9.

12 Conclusions and discussion

In this thesis we made the translation of the two mathematical books from Chekroun et al[4, 5] to an application. We showed how the PM method is connected to the Galerkin in the deterministic case and explained how the PM method works in the deterministic and stochastic case. Further this thesis gives an easy introduction on how to work with the PM method.

Our first research question was: how does the parameterising manifold method perform compared to a Galerkin method in the deterministic case? We showed how the Galerkin and the PM method are related to each other and that the PM method may be seen as the extension of a Galerkin method, in the sense that the Galerkin method with m variables is the PM method with m resolved variables and without unresolved variables.

We observed that for $R = 37$ and a perturbation in only one eigenvector the PM approach was already able to give a reasonable approximation of the full model. Here the evolution of the amplitude of the first eigenvector was described by a third order polynomial. The Galerkin method is for $R = 37$ able to give a good reduced model when the perturbation was expanded in two eigenvectors. Here the evolution of the amplitudes was described by a coupled second order polynomial.

Generally speaking we need less 'resolved' variables for the PM method, but the evolution equations for the PM method are described by a system of coupled fourth order polynomials. For the Galerkin method we need maybe more 'variables', but the evolution equations are described by a system of coupled second order polynomials. We did not study the efficiency of the PM method compared to the Galerkin method: this is a point for further research.

Our other research question was: are the stochastic reduced models capable of capturing important features of the full model? We observed that this is the case. For example we observed that 0 was a trap for both the reduced and full model and we observed that if the amplitude of the stochastic noise passed a certain threshold that then the reduced model and the full model would eventually reach 0 and remain there. Furthermore we were able to make PDFs with the full model which seem to capture the dynamics of the full model well.

13 Outlook

It will be interesting to apply this method to a (supercritical) Hopf bifurcation and to see if we can obtain a stochastic reduced model which captures the Hopf bifurcation. Another interesting question is, how far away (in the sense of the bifurcation parameter R) from the (pitchfork) bifurcation are we still able to obtain a good reduced model?
The approach we followed here with the multiplicative noise is interesting if the perturbation is started from an unstable stationary state. If we would start from a stable stationary state then our perturbation would quickly decay to zero, and if the perturbation is zero it remains zero because of the multiplicative noise used. Therefore studying stable stationary states with this model is not interesting.

If we consider a full stochastic model purely driven by additive noise (think for example of noise in the wind forcing) it is possible to get a reduced stochastic model which includes additive noise. For how to obtain such a model see [3]. With such a model it will be interesting to study PDFs around stable stationary states, because the perturbation can no longer be caught in 0. It is interesting to make PDFs for different parameter values each time closer to a bifurcation and to see how the PDF changes if we approach a bifurcation. An interesting question is if the deformation of the PDF will be bifurcation specific: with this we mean that we can predict from how the PDF changes shape that a bifurcation will happen, and what kind of bifurcation will happen.

Further if we would use a model which includes additive noise, we should be able to see jumping between the two stable states of the supercritical pitchfork bifurcation for a high enough value of additive noise and we should be able to plot a PDF in which this is visible. For the supercritical pitchfork bifurcation in the additive noise case with $m = 1$, we will probably get something like in [8, Sect. 4.3.2].

An interesting application will be to apply the PM method to stochastic models which describe three dimensional currents.

13.1 Acknowledgements

I want to thank my supervisors Henk Dijkstra and Jason Frank for their many useful remarks and for the nice cooperation. Further I want to thank Mickaël D. Chekroun who helped me a lot during the week he was in the Netherlands. He showed that there was an analytical expression of a parameterising manifold available and later also helped me with some very useful comments to explain the PM method. Further I want to thank all the students of the IMAU student room for useful conversations, motivating each other, have nice chats about all kind of subjects and the lunch walks and other fun stuff we did together. Without them I am not sure if I could find the motivation to work on my thesis every day during this nine months. I want to thank Jason Frank and Stefan Korenberg for reading preliminary versions of my thesis and giving many useful remarks on the content and on the English used.

References

[1] M. D. Chekroun. Private communication.

[2] M. D. Chekroun and H. Liu. Finite-horizon parameterizing manifolds, and applications to suboptimal control of nonlinear parabolic PDEs. *Acta Applicandae Mathematicae*, 135(1):81–144, 2015.

[3] M. D. Chekroun, H. Liu, and S. Wang. Non-markovian reduced systems for stochastic partial differential equations: The additive noise case. *arXiv preprint arXiv:1311.3069*, 2013.

[4] M. D. Chekroun, H. Liu, and S. Wang. *Approximation of Stochastic Invariant Manifolds: Stochastic Manifolds for Nonlinear SPDEs I*. Springer, 2015.

[5] M. D. Chekroun, H. Liu, and S. Wang. *Stochastic Parameterizing Manifolds and Non-Markovian Reduced Equations: Stochastic Manifolds for Nonlinear SPDEs II*. Springer, 2015.

[6] H. A. Dijkstra. *Nonlinear physical oceanography: a dynamical systems approach to the large scale ocean circulation and El Nino*, volume 28. Springer Science & Business Media, 2005.

[7] H. A. Dijkstra. *Dynamical oceanography*. Springer Science & Business Media, 2008.

[8] H. A. Dijkstra. *Nonlinear climate dynamics*. Cambridge University Press, 2013.

[9] H. A. Dijkstra and C. A. Katsman. Temporal variability of the wind-driven quasi-geostrophic double gyre ocean circulation: Basic bifurcation diagrams. *Geophysical & Astrophysical Fluid Dynamics*, 85(3-4):195–232, 1997.

[10] G. Golub and C. v. Loan. Matrix computations. *Johns Hopkins series in mathematical sciences (3)*, 1983.

[11] M. Golubitsky, I. Stewart, et al. *Singularities and groups in bifurcation theory*, volume 2. Springer Science & Business Media, 2012.

[12] H. B. Keller. Numerical solution of bifurcation and nonlinear eigenvalue problems. *Applications of bifurcation theory*, pages 359–384, 1977.

[13] P. E. Kloeden and E. Platen. Numerical solution of stochastic differential equations springer-verlag. *New York*, 1992.

[14] D. Kondrashov, M. D. Chekroun, and M. Ghil. Data-driven non-Markovian closure models. *Physica D.*, 297:33–55, 2015.

[15] Y. Saad. *Iterative methods for sparse linear systems*. Siam, 2003.

[16] P. C. van der Vaart, H. M. Schuttelaars, D. Calvete, and H. A. Dijkstra. Instability of time-dependent wind-driven ocean gyres. *Physics of Fluids (1994-present)*, 14(10):3601–3615, 2002.